

The Effects of Cold Dark Matter Decoupling and Pair Annihilation on Cosmological Perturbations

Edmund Bertschinger

Department of Physics, MIT Room 37-602A, 77 Massachusetts Ave., Cambridge, MA 02139

Weakly interacting massive particles are part of the lepton-photon plasma in the early universe until kinetic decoupling, after which time the particles behave like a collisionless gas with nonzero temperature. The Boltzmann equation for WIMP-lepton collisions is reduced to a Fokker-Planck equation for the evolution of the WIMP distribution including scalar density perturbations. This equation and the Einstein and fluid equations for the plasma are solved numerically including the acoustic oscillations of the plasma before and during kinetic decoupling, the frictional damping occurring during kinetic decoupling, and the free-streaming damping occurring afterwards and throughout the radiation-dominated era. An excellent approximation reduces the solution to quadratures for the cold dark matter density and velocity perturbations. The subsequent evolution is followed through electron pair annihilation and the radiation-matter transition; analytic solutions are provided for both large and small scales. For a 100 GeV WIMP with bino-type interactions, kinetic decoupling occurs at a temperature $T_d = 16$ MeV. The transfer function in the matter-dominated era leads to an abundance of small cold dark matter halos; with a smooth window function the Press-Schechter mass distribution is $dn/d\ln M \propto M^{-1/3}$ for $M < 10^{-4} (T_d/10 \text{ MeV})^{-3} M_\odot$.

PACS numbers: 95.35.+d, 95.30.Cq, 98.80.-k, 98.80.Cq, 05.10.Gg

I. INTRODUCTION

Weakly interacting massive particles (WIMPs) are perhaps the leading candidate for the cold dark matter (CDM) making up most of the nonrelativistic mass density of the universe today [1]. Although candidate WIMPs are 10 to 1000 times more massive than nucleons and have no electromagnetic or color charges, their cosmic histories share many parallels with nucleons. After their abundances froze out at $\sim 10^{-10}$ the number density of photons, both WIMPs and nucleons remained thermally coupled to the plasma by elastic scattering with abundant relativistic particles. Acoustic oscillations in the relativistic plasma imprinted oscillations on both WIMPs and nucleons. Eventually the plasma released its grip on both types of particles. For WIMPs, this event is called kinetic decoupling; for nucleons, recombination.

During kinetic decoupling, friction between the WIMP gas and relativistic plasma led to Silk damping of small-scale waves similar to what happened much later for atomic matter at recombination. After the respective decoupling periods ended, pressure forces (and in the case of WIMPs, shear stress) inhibited gravitational instability on small scales. Still later, both WIMPs and nucleons played a major role in galaxy formation.

There are, of course, significant differences between the cosmic evolution of WIMPs and nucleons. Most evident are the quantitative differences: because their interactions are so weak, WIMPs decoupled from the plasma less than one second after the big bang. Consequently the WIMP acoustic oscillations appear only on a length scale vastly smaller (\sim parsec scales) than the baryon acoustic oscillations. The physics of nucleon decoupling, as imprinted in the galaxy distribution [2] and in the cosmic microwave background radiation [3] provides a powerful probe of cosmic parameters and inflationary cosmology.

If it were possible to similarly measure fluctuations on the scale of WIMP acoustic oscillations, we would have a dramatic consistency test of the cosmological model as well as an astrophysical measurement of WIMP properties.

One way to constrain the parameters of cold dark matter decoupling is to measure the mass function of the smallest dark matter clumps today [4, 5, 6]. Such clumps would be far too diffuse to host observable concentrations of atomic matter. However, they might be observable through the products of the very rare WIMP-WIMP annihilations taking place in the cores of these objects. Diemand *et al.* [7] proposed that numerous Earth-mass clumps might survive to the present day and provide a detectable gamma-ray signal. The mass and abundance of these clumps depends on cosmic fluctuation evolution during and after kinetic decoupling.

WIMPs and nucleons also differ in a qualitative manner which has important consequences for the evolution of fluctuations through kinetic decoupling. After recombination, elastic scattering is rapid enough for atoms (and the residual free electrons) to behave as a nearly perfect gas on cosmological scales. Baryons behave like a fluid. WIMPs, however, collide too infrequently to thermalize after kinetic decoupling. WIMPs behave like a collisionless gas. Different approximations to the evolution of this collisionless gas have led to different results for the small-scale transfer function of CDM fluctuations [6, 8, 9].

In the present paper, the transfer functions for CDM fluctuations are calculated starting from the full Boltzmann equation describing elastic scattering between WIMPs and the relativistic leptons present before neutrino decoupling and electron-positron pair annihilation. Because the momentum transfer per collision with non-relativistic WIMPs is small, the Boltzmann equation reduces to the Fokker-Planck equation describing dif-

fusion in velocity space caused by elastic scattering, combined with advection and gravitational forces. The Fokker-Planck equation fully describes kinetic decoupling and the evolution of perturbations of any length scale without approximating the WIMPs either as a perfect fluid or fully collisionless gas. Although the solution of the perturbed Fokker-Planck equation is more difficult than the solution of coupled fluid and collisionless Boltzmann equations, it is both numerically and analytically tractable (with an excellent approximation) in the present case.

After kinetic decoupling, two additional events have an effect on the CDM transfer function. The first is electron-positron pair annihilation, which changes the equation of state of the plasma thereby modifying the evolution of fluctuations. Although the effects are small, they can be analytically calculated. The more important event is the transition from a radiation- to matter-dominated universe occurring about 10^5 years after the big bang. If the photons and neutrinos are treated as fluids, it is possible to get analytic results for the linear evolution all the way to low redshift which are accurate to a few percent. With these results in place, using standard techniques it is straightforward to estimate the mass function of CDM clumps at high redshift.

II. EVOLUTION OF WIMP PERTURBATIONS THROUGH KINETIC DECOUPLING

Weakly interacting dark matter particles are described by their phase space density, which obeys the Boltzmann equation governing transport by collisions with leptons (during kinetic decoupling these are just electrons, positrons, and neutrinos). For definiteness we will take the WIMP to be the lightest neutralino χ^0 , however the results are easily applied to other WIMP candidates by modifying the scattering matrix element below.

Let $f_\chi(\mathbf{p})$ and $f_L(\mathbf{p})$ be the proper phase space densities of neutralinos and ultrarelativistic leptons, respectively, where \mathbf{p} is the proper three-momentum in a local orthonormal frame. (The spacetime coordinates \mathbf{x} and t are suppressed for brevity.) The phase space densities are normalized so that $\int f(\mathbf{p}) d^3p$ is the spatial number density, summed over spin states (we assumed unpolarized spins). One distribution function suffices for the relativistic leptons because electroweak interactions maintain local thermal equilibrium at a temperature T_L . Elastic scattering of neutralinos and leptons cause the neutralino distribution to evolve according to the Boltzmann equation,

$$p_1^\mu \partial_\mu f_{1\chi} = \int \frac{d^3 p_2}{E_2} \int \frac{d^3 p_3}{E_3} \int \frac{d^3 p_4}{E_4} \left| \frac{\mathcal{M}}{8\pi} \right|^2 \times \delta^4(p_1 + p_2 - p_3 - p_4) \times \left[f_{3\chi} f_{4L} (1 - \tilde{f}_{2L}) - f_{1\chi} f_{2L} (1 - \tilde{f}_{4L}) \right], \quad (1)$$

where \mathcal{M} is the Lorentz-invariant scattering amplitude,

$f_{1\chi} \equiv f_\chi(\mathbf{p}_1)$ and similarly for the other distribution functions, E_i is the energy of particle i , and $\tilde{f}_L \equiv (2\pi\hbar)^3 f_L/2$ is the occupation number. Pauli blocking must be included for the leptons but not for the neutralinos since the latter have a low density after chemical decoupling. Equation (1) is relativistically covariant but gives only the effects of collisions; the effects of gravitational perturbations will be added later. Assuming effectively massless leptons, the matrix element for slepton exchange is given in Appendix A of [4] and may be written

$$|\mathcal{M}|^2 = C \frac{p_{\text{CM}}^2}{m_\chi^2} \left(1 - \frac{t_{\text{M}}}{4p_{\text{CM}}^2} \right), \quad (2)$$

where

$$C = 256 \sum_L (b_L^4 + c_L^4) \left(\frac{G_F m_W^2 m_\chi^2}{m_L^2 - m_\chi^2} \right)^2 \quad (3)$$

is a dimensionless constant depending on the relevant particle masses and couplings (G_F is the Fermi constant, b_L and c_L are left and right chiral vertices, and m_W , m_L , and m_χ are respectively the masses of the W boson, the slepton, and the neutralino; $G_F m_W^2 = 0.0754$). Here we assume following Ref. [4] that the neutralino is a pure bino. Additionally, p_{CM} is the momentum in the center of momentum frame, and (using metric signature $-+++$) $t_{\text{M}} = -(p_2 - p_4)^2 = -2p_{\text{CM}}^2(1 - \cos\theta_{\text{CM}})$ is one of the Mandelstam variables.

For $p_{\text{CM}} \sim T_L \ll m_\chi$, $p_{\text{CM}} = m_\chi \epsilon [1 - \epsilon + \frac{3}{2}\epsilon^2 + O(\epsilon^3)]$ where $\epsilon \equiv -p_3 \cdot p_4 / m_\chi^2$. In the lab frame, working to first order in T_L/m_χ , assuming $p_1 \sim \sqrt{m_\chi T_L}$, the collision kinematics gives

$$\frac{1 - \cos\theta_{\text{CM}}}{1 - \mathbf{n}_2 \cdot \mathbf{n}_4} = 1 + \frac{(\mathbf{n}_2 + \mathbf{n}_4) \cdot (\mathbf{p}_1 + \mathbf{p}_2)}{m_\chi} + \left(\frac{p_1}{m_\chi} \right)^2 (\mu_{12}^2 + \mu_{12}\mu_{14} + \mu_{14}^2 - 1), \quad (4)$$

where $\mu_{ij} = \mathbf{n}_i \cdot \mathbf{n}_j$ and $\mathbf{n}_i = \mathbf{p}_i/p_i$. Another useful relation follows from energy conservation,

$$\frac{p_4}{p_2} = 1 + \frac{p_1}{m_\chi} (\mu_{14} - \mu_{12}) \left(1 + \frac{p_1}{m_\chi} \mu_{14} \right) + \frac{p_2}{m_\chi} (\mu_{24} - 1), \quad (5)$$

valid again to first order in T_L/m_χ .

Frequent collisions among the leptons maintain thermal equilibrium. Assuming negligible chemical potential, for each species of massless lepton we have

$$[\tilde{f}_L(\mathbf{p})]^{-1} = 1 + \exp \left[\frac{p}{T_L} (1 - \mathbf{n} \cdot \mathbf{v}_L) \right], \quad (6)$$

where \mathbf{v}_L is the (very small) local lepton fluid velocity due to cosmological perturbations. It is easy to check that an equilibrium solution of (1) is then the Maxwell-Boltzmann distribution with mean velocity \mathbf{v}_L .

For $T_L \ll m_\chi$ the term $f_{3\chi}$ may be Taylor-expanded in (1). After a lengthy calculation using (4)–(6), one obtains $p^\mu \partial_\mu f = m_\chi (df/dt)_c$ (dropping the subscript on f_χ) where the Boltzmann collision integral becomes the Fokker-Planck operator,

$$\left(\frac{df}{dt} \right)_c = \gamma \frac{\partial}{\partial \mathbf{p}} \cdot \left[(\mathbf{p} - m_\chi \mathbf{v}_L) f + m_\chi T_L \frac{\partial f}{\partial \mathbf{p}} \right], \quad (7)$$

where

$$\gamma = \frac{155\pi^3 C T_L^6}{6048 m_\chi^5} \quad (8)$$

is a rate coefficient (in units where $\hbar = c = 1$). Our exact result for the rate coefficient is larger by a factor 9.9 than the estimate obtained from Eqs. (9) and (12) of Ref. [4] and by a factor 14.5 than Eq. (17) of Ref. [5]. The rate is greater than the simple estimates made in previous work because of the details of the kinematics and the near-cancelation of forward and inverse rates in (1). A larger rate coefficient leads to a lower temperature for kinetic decoupling than previous estimates.

If we neglect spatial inhomogeneities, the unperturbed phase space density $f_0(q, \tau)$ depends on both comoving momentum $q = a\mathbf{p}$ and conformal time τ according to

$$\frac{\partial f_0}{\partial \tau} = \gamma a \frac{\partial}{\partial \mathbf{q}} \cdot \left[\mathbf{q} f_0 + a^2 m_\chi T_L \frac{\partial f_0}{\partial \mathbf{q}} \right]. \quad (9)$$

Amazingly, for any time-dependence of γ , a , and T_L an exact solution to this Fokker-Planck equation is the Maxwell-Boltzmann distribution

$$f_0(q, \tau) = \frac{\exp(-q^2/2\sigma_q^2)}{(2\pi\sigma_q^2)^{3/2}}, \quad \sigma_q(\tau) = a(\tau) \sqrt{m_\chi T_\chi(\tau)}, \quad (10)$$

where the WIMP temperature T_χ follows from integrating

$$\frac{d \ln(a^2 T_\chi)}{d\tau} = 2\gamma a \left(\frac{T_L}{T_\chi} - 1 \right). \quad (11)$$

During adiabatic evolution in the early universe, $T_L \propto a^{-1} \propto \tau^{-1}$ and the WIMP proper temperature is then given in terms of the incomplete Gamma function by

$$T_\chi(\tau) = T_L s^{1/4} e^s \Gamma(\frac{3}{4}, s), \quad s \equiv \frac{1}{2} \gamma a \tau = \frac{\gamma}{2H}. \quad (12)$$

Equation (10) may be multiplied by any constant, allowing the comoving number density of WIMPs to be normalized to its value after freeze-out.

Familiarity with Brownian motion makes it seem natural that the solution to the Fokker-Planck equation is a Maxwell-Boltzmann distribution. However, the lepton temperature T_L and the momentum transfer rate γ are falling with time and WIMP-WIMP elastic scattering is far too slow to thermalize the distribution. Even

so, collisions with the leptons maintain the WIMPs in a thermal distribution with a temperature that deviates increasingly from the lepton temperature throughout kinetic decoupling. Once kinetic decoupling is complete the WIMP momenta redshift as $p \propto a^{-1}$ preserving the Maxwell-Boltzmann distribution with $T_\chi \propto a^{-2}$.

Long before kinetic decoupling ($s \gg 1$), $T_\chi/T_L = 1 - 1/(4s) + O(s^{-2})$. After kinetic decoupling ($s < 1$), $T_\chi/T_L \rightarrow \Gamma(\frac{3}{4})s^{1/4} \propto a^{-1}$. Defining the kinetic decoupling time by $s = 1$ yields

$$\begin{aligned} T_d &\equiv T_L(s=1) = 1.430 C^{-1/4} g_{\text{eff}}^{1/8} \left(\frac{m_\chi^5}{m_{\text{Pl}}} \right)^{1/4} \\ &= 7.650 C^{-1/4} g_{\text{eff}}^{1/8} \left(\frac{m_\chi}{100 \text{ GeV}} \right)^{5/4} \text{ MeV}. \end{aligned} \quad (13)$$

For typical SUSY masses, kinetic decoupling occurs after muon annihilation when the only abundant leptons are electron pairs and neutrinos, for which (with $\sin^2 \theta_W = 0.223$) $\sum_L (b_L^4 + c_L^4) = 4 \tan^2 \theta_W = 1.15$ and $g_{\text{eff}} = 43/4$. With $m_\chi = 100$ GeV and $m_{\tilde{L}} = 200$ GeV, $C = 0.186$ yielding $T_d = 15.7$ MeV. Profumo *et al.* [10] show that T_d can span the range from a few MeV to a few GeV for reasonable WIMP models. Here we take the supersymmetric bino as a candidate but will show how numerical results scale with T_d .

Next we examine the effect of density, velocity, and gravitational potential fluctuations during kinetic decoupling. The perturbed phase space density is $f(\mathbf{x}, \mathbf{q}, \tau)$, where \mathbf{x} are comoving spatial coordinates, $\mathbf{q} = a\mathbf{p}$ are the conjugate momenta, and τ is conformal time. The perturbed line element in conformal Newtonian gauge is written $ds^2 = a^2[-(1 + 2\Phi)d\tau^2 + (1 - 2\Psi)d\mathbf{x} \cdot d\mathbf{x}]$. Including the effects of the metric perturbations Φ and Ψ , the Boltzmann equation becomes

$$\frac{\partial f}{\partial \tau} + \mathbf{v} \cdot \frac{\partial f}{\partial \mathbf{x}} + \left(\dot{\Psi} \mathbf{q} - \epsilon \frac{\partial \Phi}{\partial \mathbf{x}} \right) \cdot \frac{\partial f}{\partial \mathbf{q}} = a \left(\frac{df}{dt} \right)_c, \quad (14)$$

where $\mathbf{v} = \mathbf{q}/\epsilon$ is the proper velocity measured by a comoving observer, $\epsilon \equiv (q^2 + a^2 m_\chi^2)^{1/2}$ is the comoving energy, and $\mathbf{q} = q\mathbf{n}$. With comoving variables, the Fokker-Planck operator becomes

$$a \left(\frac{df}{dt} \right)_c = \gamma a \frac{\partial}{\partial \mathbf{q}} \cdot \left[(\mathbf{q} - \mathbf{q}_L) f + a^2 m_\chi T_L \frac{\partial f}{\partial \mathbf{q}} \right], \quad (15)$$

where $\mathbf{q}_L \equiv a m_\chi \mathbf{v}_L \equiv -a m_\chi \nabla u_L$.

Now we linearize (15) for first-order perturbations of the lepton fluid by writing $T_L \rightarrow T_L(\tau) + T_1(\mathbf{x}, \tau)$. The fields $T_1(\mathbf{x}, \tau)$, $\Phi(\mathbf{x}, \tau)$, $\Psi(\mathbf{x}, \tau)$, and the lepton velocity potential $u_L(\mathbf{x}, \tau)$ are treated as first-order quantities. Assuming $v^2 \ll 1$ and performing a spatial Fourier transform, we obtain the linear perturbation equation

$$\begin{aligned} \frac{1}{f_0} \left[\left(\frac{\partial f}{\partial \tau} \right)_q + i(\mathbf{k} \cdot \mathbf{v}) f - \gamma a L_{\text{FP}} f \right] \\ = \dot{\Psi} \frac{q^2}{\sigma_q^2} - \frac{i\mathbf{k} \cdot \mathbf{q}}{a T_\chi} (\Phi + \gamma a u_L) + \gamma a \left(\frac{q^2}{\sigma_q^2} - 3 \right) \frac{T_1}{T_\chi}, \end{aligned} \quad (16)$$

where

$$L_{\text{FP}} f \equiv \frac{\partial}{\partial \mathbf{q}} \cdot \left(\mathbf{q} f + a^2 m_\chi T_L \frac{\partial f}{\partial \mathbf{q}} \right) . \quad (17)$$

After WIMP freeze-out, the leptons dominate the gravitational potentials so that $\dot{\Psi}$, Φ , u_L , and T_1 are functions of (\mathbf{k}, τ) given by the solution for a perfect relativistic fluid. Equation (16) generalizes the collisionless Boltzmann equation of Ref. [11] to include the effects of dark matter collisions with relativistic leptons.

To integrate (16) for the phase space density f we will expand the momentum dependence in eigenfunctions of the Fokker-Planck operator L_{FP} :

$$L_{\text{FP}} \phi_{nlm} = -(2n+l) \phi_{nlm} , \quad (18a)$$

$$\phi_{nlm} = e^{-y} y^{l/2} L_n^{(l+1/2)}(y) Y_{lm}(\mathbf{n}) . \quad (18b)$$

Here $y \equiv q^2/(2a^2 m_\chi T_L)$ and $L_n^{(\alpha)}(y)$ is a generalized Laguerre polynomial, also known as a Sonine polynomial. It is defined by the following series expansion:

$$L_n^{(\alpha)}(x) = \sum_{k=0}^n \frac{\Gamma(n+\alpha+1)}{\Gamma(k+\alpha+1)} \frac{(-x)^k}{k!(n-k)!} . \quad (19)$$

Generalized Laguerre polynomials have orthonormality relation

$$\int_0^\infty \frac{n! x^\alpha e^{-x}}{\Gamma(n+\alpha+1)} L_n^{(\alpha)}(x) L_{n'}^{(\alpha)}(x) dx = \delta_{nn'} \quad (20)$$

and completeness relation

$$\sum_{n=0}^\infty \frac{n! (xx')^{\alpha/2} e^{-(x+x')/2}}{\Gamma(n+\alpha+1)} L_n^{(\alpha)}(x) L_n^{(\alpha)}(x') = \delta(x-x') . \quad (21)$$

We will expand the phase space density $f(\mathbf{k}, \mathbf{q}, \tau)$ in the complete set ϕ_{nlm} . However, it is unnecessary to include all (nlm) in this expansion. Prior to kinetic decoupling the Fokker-Planck operator L_{FP} rapidly damps all terms except ϕ_{000} and those terms that are induced by the right-hand side of (16). The rotational symmetry of this equation implies that only the $m = 0$ terms are induced, where the polar axis for the spherical harmonics is given by $\hat{\mathbf{k}} = \mathbf{k}/k$ [22]. Thus we may write

$$\begin{aligned} f(\mathbf{k}, \mathbf{q}, \tau) &= \frac{e^{-y}}{(2\pi a^2 m_\chi T_L)^{3/2}} \\ &\times \sum_{n,l=0}^\infty (-i)^l (2l+1) S_{nl}(y) P_l(\hat{\mathbf{k}} \cdot \mathbf{n}) f_{nl}(\mathbf{k}, \tau) , \\ S_{nl} &\equiv y^{l/2} L_n^{(l+1/2)}(y) . \end{aligned} \quad (22)$$

Before writing the perturbation equations, let us examine the unperturbed solution, $f = f_0(q, \tau) \delta^3(\mathbf{k})$. The exponential factors differ in (10) and (22), implying that

the Laguerre expansion includes more than one term. Indeed, one finds

$$f = f_0(q, \tau) \Rightarrow f_{nl} = \delta_{l0} \left(1 - \frac{T_\chi}{T_L} \right)^n . \quad (23)$$

Prior to kinetic decoupling, when collisions maintain $T_\chi = T_L$, $f_{00} = 1$ and the other coefficients vanish. After kinetic decoupling, $f_{n0} \rightarrow 1$ for all n . The Laguerre expansion must be carried to high order in order to convert e^{-y} to $\exp(-q^2/2\sigma_q^2)$. Similarly, we should expect the perturbed phase space density also to require many terms in n after kinetic decoupling.

Substituting (22) into (16) and using orthonormality and several recurrence relations for the generalized Laguerre polynomials, we obtain a system of coupled ordinary differential equations for the evolution of the perturbed phase space density,

$$\begin{aligned} \dot{f}_{nl} + (2n+l)(\gamma a + R) f_{nl} - 2nR f_{n-1,l} \\ + k \sqrt{\frac{2T_L}{m_\chi}} \left\{ \left(\frac{l+1}{2l+1} \right) [(n+l+\frac{3}{2}) f_{n,l+1} - n f_{n-1,l+1}] \right. \\ \left. + \frac{l}{2l+1} (f_{n+1,l-1} - f_{n,l-1}) \right\} \\ = \delta_{l0} [3\dot{\Psi} A_n - 2(\dot{\Psi} + \gamma a T_1/T_\chi) B_n] \\ + \delta_{l1} \frac{k}{3} \sqrt{\frac{2m_\chi}{T_0}} (\Phi + \gamma a u_L) A_n , \end{aligned} \quad (24)$$

where

$$\begin{aligned} R &\equiv \frac{d}{d\tau} \ln(a T_L^{1/2}) , \\ A_n(\tau) &\equiv \left(1 - \frac{T_\chi}{T_L} \right)^n , \\ B_n(\tau) &\equiv n \left(\frac{T_\chi}{T_L} \right) \left(1 - \frac{T_\chi}{T_L} \right)^{n-1} . \end{aligned} \quad (25)$$

The density perturbation is $\delta(\mathbf{k}, \tau) = f_{00}$ for $\mathbf{k} \neq 0$.

The source terms for Eqs. (24) are provided by the relativistic plasma. Their time-dependence changes during lepton pair annihilation and neutrino decoupling. For reasonable parameters, neutralino kinetic decoupling occurs after muon annihilation but before electron annihilation and neutrino decoupling. During this era, the isentropic mode of perturbations has time-dependence given by the relativistic perfect-fluid transfer functions

$$\Phi = \Psi = -\frac{3}{\theta^3} (\sin \theta - \theta \cos \theta) , \quad (26a)$$

$$\mathcal{H} u_L = -\frac{3}{2\theta} \left[\left(1 - \frac{2}{\theta^2} \right) \sin \theta + \frac{2}{\theta} \cos \theta \right] , \quad (26b)$$

$$\frac{T_1}{T_L} = \frac{\delta_L}{3} = -\frac{\theta^2}{2} \Phi - \mathcal{H} u_L , \quad (26c)$$

where $\mathcal{H} \equiv \dot{a}/a$, $\theta \equiv k\tau/\sqrt{3}$, and the transfer functions are normalized so that $\Phi = -1$ for $\theta = 0$ [23]. The actual perturbations are obtained by multiplying the transfer

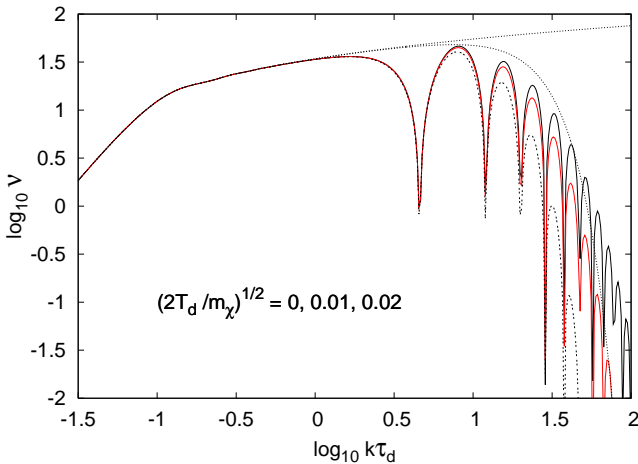


FIG. 1: CDM density transfer function versus wavenumber at conformal time $\tau = 72\tau_d$. The three oscillating curves assume that kinetic decoupling occurred at τ_d for three different values of the radiation temperature T_d relative to the CDM particle mass m_χ ; the amplitude of the oscillations decreases with increasing T_d/m_χ . The upper, monotonic curve assumes that the CDM is always collisionless and was never coupled to the radiation. The other non-oscillating curve shows a crude model of kinetic decoupling described by a Gaussian cutoff.

functions with the scalar field $\Psi_0(\mathbf{k})$ that gives the spatial dependence of the initial (inflationary) curvature fluctuations. As the inflationary curvature perturbations are well known (a Gaussian random field with nearly scale-invariant spectral density $P \propto k^{-3}$), here we work with transfer functions.

Initial conditions for Eqs. (24) are obtained by examining the solutions for $s = \frac{1}{2}\gamma a\tau \equiv (\tau/\tau_d)^{-4} \gg 1$. Isentropic initial conditions have $f_{00} = \delta = \delta_L$. The only significantly perturbed components of f for the strongly coupled plasma are the thermal equilibrium values

$$f_{00} = \delta_L, \quad f_{01} = \frac{k}{3} \sqrt{\frac{2m_\chi}{T_L}} u_L, \quad f_{10} = -\frac{T_1}{T_L} = -\frac{1}{3} \delta_L. \quad (27)$$

All other components f_{nl} are kept small by rapid WIMP-lepton collisions. Equations (24) with $n \leq 1400$ and $l \leq 15$ were integrated to $\tau = 72\tau_d$ using the standard explicit ODE solver DVERK. Convergence testing showed that higher-order terms in the Laguerre expansion were negligible.

Figure 1 shows the results for the density transfer function expressed using the gauge-invariant variable ν , defined as the CDM number density perturbation in a synchronous gauge for which the mean CDM velocity vanishes in the coordinate frame (for a nonrelativistic particle, ν equals Bardeen's variable ϵ_m). This variable, which is used by CMBFAST [12], is related to the conformal Newtonian gauge variables by

$$\nu \equiv \delta + 3\mathcal{H}u. \quad (28)$$

For wavelengths longer than the radiation acoustic length $\tau/\sqrt{3}$, $\nu = \delta_L + 3\mathcal{H}u_L \approx \frac{1}{2}(k\tau)^2$. For wavelengths shorter than the radiation acoustic length at τ but longer than the acoustic length at τ_d (i.e., $10\tau^{-1} < k < \tau_d^{-1}$), the acoustic oscillations of the gravitational potential average out leading to a suppression of growth induced in the CDM. For these intermediate wavelengths the transfer function is a logarithmic function of wavenumber. If the dark matter were completely non-interacting, this logarithm would continue to arbitrarily high wavenumbers, as illustrated by the monotonically rising curve in Fig. 1.

Because WIMP dark matter was collisionally coupled to the relativistic lepton plasma at early times, the CDM transfer function in Fig. 1 shows remnant damped acoustic oscillations at short wavelengths. For comparison a Gaussian transfer function is shown, with no oscillations. In this model, the effects of kinetic decoupling are described by multiplying the transfer function for the completely non-interacting case by $\exp(-k^2/2\sigma_k^2)$. As we will see, a simple model of free streaming predicts that $(\sigma_k \tau_d)^{-1} \approx [\Gamma(\frac{3}{4}) T_d/m_\chi]^{1/2} [\ln(\tau/\tau_d)]$ during the radiation-dominated era. For $\tau = 72\tau_d$ and $(2T_d/m_\chi)^{1/2} = 0.01$ this model would predict $\sigma_k \tau_d \approx 30$ whereas the curve shown in Fig. 1 has $\sigma_k \tau_d = 18$. Free-streaming does not give a good approximation to the actual transfer function.

The exact transfer functions shown in Fig. 1 decrease less rapidly with wavenumber than the approximate transfer functions of Ref. [9] which were computed using a fluid approximation followed by free-streaming. The following section reviews the free-streaming solution and then develops a more accurate approximation based on moments of the exact Fokker-Planck equation.

III. APPROXIMATE DESCRIPTIONS OF PERTURBATION EVOLUTION THROUGH KINETIC DECOUPLING

In this section we consider two different approximations which provide analytical insight to the numerical solution of the Fokker-Planck equation. The CDM behaves at early times like a fluid and at late times like a free-streaming collisionless gas, and in these limits we can develop useful analytical approximations.

A. Free-streaming model

For $\tau \gg \tau_d$, the terms proportional to γa may be dropped in (16). The differential equation may then be integrated to give $f(\mathbf{k}, \mathbf{q}, \tau)$ in terms of the initial value $f(\mathbf{k}, \mathbf{q}, \tau_*)$ for any $\tau_* \gg \tau_d$. Integrating over momenta gives the conformal Newtonian gauge density perturba-

tion,

$$\delta(\mathbf{k}, \tau) = \int d^3q e^{-i\zeta\mathbf{k}\cdot\mathbf{q}} f(\mathbf{k}, \mathbf{q}, \tau_*) + \int_{\tau_*}^{\tau} d\tau' e^{-M'/2} \times \left[(3 - M') \dot{\Psi}(\mathbf{k}, \tau') + k^2 \tau' \ln\left(\frac{\tau}{\tau'}\right) \Phi(\mathbf{k}, \tau') \right], \quad (29)$$

where we have assumed evolution in the radiation-dominated era with

$$\zeta \equiv \frac{\tau_*}{a_* m_\chi} \ln\left(\frac{\tau}{\tau_*}\right), \quad M' \equiv \frac{T'_\chi}{m_\chi} (k\tau')^2 \ln^2\left(\frac{\tau}{\tau'}\right). \quad (30)$$

For large spatial frequencies, $k\tau \gg 1$, the gravitational potentials — which are dominated by relativistic particles — oscillate rapidly leading to a small net integral contribution; ignoring this, $\delta(\mathbf{k}, \tau)$ is a momentum-space Fourier transform of the distribution function at the initial time τ_* .

Obtaining the exact solution still requires numerical integration of (16) through kinetic decoupling, or equivalently, integrating the system of equations (24). However, we can get an idea of the effects of free-streaming by making an instantaneous decoupling approximation, treating the CDM as a fluid with a Maxwell-Boltzmann velocity distribution for $\tau < \tau_*$ and by (29) for $\tau > \tau_*$, as was done in Ref. [9]. Then, whether or not the CDM is strongly coupled to the radiation, the perturbed distribution function is fully specified by the perturbations of density, temperature, and velocity $\mathbf{v} = -i\mathbf{k}u$,

$$\delta f = f_0(q, \tau) \left[\frac{\delta\rho}{\rho} + \frac{1}{2} \left(\frac{q^2}{\sigma_q^2} - 3 \right) \frac{\delta T_\chi}{T_\chi} - \frac{i u \mathbf{k} \cdot \mathbf{q}}{a T_\chi} \right]. \quad (31)$$

Carrying out the Fourier transform in (29) now yields

$$\delta(\tau) = e^{-M/2} \left[\left(\delta - \frac{M}{2} \frac{\delta T_\chi}{T_\chi} \right)_{\tau_*} - k^2 \tau_* u(\tau_*) \ln\left(\frac{\tau}{\tau_*}\right) \right], \quad (32)$$

where wavenumber arguments have been dropped for brevity, and

$$M \equiv \frac{k^2}{k_f^2} \ln^2\left(\frac{\tau}{\tau_*}\right), \quad k_f^{-2} = \frac{\tau_*^2 T_\chi(\tau_*)}{m_\chi} = \Gamma\left(\frac{3}{4}\right) \frac{\tau_d^2 T_d}{m_\chi}. \quad (33)$$

If $\tau_* \sim \tau_d$, then $\delta T_\chi/T_\chi \approx \frac{1}{3}\delta$; if $\tau_* \gg \tau_d$ and the fluid is approximated as being adiabatic, $\delta T_\chi/T_\chi = \frac{2}{3}\delta$.

Equation (32) corrects errors in the definition of k_f of Ref. [9] and adds the term proportional to $\delta T_\chi/T_\chi$ to their Eq. (20). This new term arises from the temperature perturbation of the CDM fluid, which modifies the distribution function and, through free-streaming, modifies the density for $\tau > \tau_*$. In particular, if the CDM perturbations are approximately adiabatic, the temperature perturbation causes the transfer function to decrease more rapidly with k .

The free-streaming solution predicts a Gaussian cutoff of the transfer function, $\delta \propto \exp(-k^2/2\sigma_k^2)$, with cutoff distance equal to the free-streaming distance,

$$\sigma_k^{-1}(\tau) = \int_{\tau_*}^{\tau} \sqrt{\frac{T_\chi}{m_\chi}} d\tau = \left[\Gamma\left(\frac{3}{4}\right) \frac{T_d}{m_\chi} \right]^{1/2} \int_{\tau_*}^{\tau} \frac{d\tau}{a/a_d}. \quad (34)$$

During the radiation-dominated era, when $a \propto \tau$, the free-streaming length grows logarithmically, but it saturates in the matter-dominated era when $a \propto \tau^2$. At first glance, Fig. 1 appears to qualitatively support the free-streaming model of a Gaussian cutoff. However, the free-streaming model predicts no damping for a super-heavy particle with $T_d/m_\chi \rightarrow 0$, while Fig. 1 shows that even in this case there is damping. This damping arises from friction between the lepton and CDM gases during decoupling (Silk damping). This friction can be accounted for by treating the CDM as an imperfect fluid.

B. Imperfect fluid model

To better describe an extended period of decoupling while allowing for small deviations from a Maxwell-Boltzmann distribution, we consider the evolution of the lowest order moments of the distribution function. We work to first order in perturbed quantities and normalize the unperturbed distribution function to $\int f_0 d^3q = 1$. The perturbations for $\mathbf{k} \neq 0$ then define the lowest-order moments

$$\begin{aligned} \int f d^3q &= \delta, \\ \int f v_j d^3q &= -i k_j u, \\ \int f v_i v_j d^3q &= (c_\chi^2 \delta + \sigma) \delta_{ij} - \frac{3}{2} (k_i k_j - \frac{1}{3} k^2 \delta_{ij}) \pi, \end{aligned} \quad (35)$$

where the density perturbation δ , velocity potential u , shear stress potential π , and entropy perturbation σ are related to our expansion coefficients by

$$\begin{aligned} \delta &= f_{00}, \quad k u = \sqrt{\frac{9 T_L}{2 m_\chi}} f_{01}, \quad k^2 \pi = \frac{5 T_L}{m_\chi} f_{02}, \\ \sigma &= \left(\frac{T_L}{m_\chi} - c_\chi^2 \right) f_{00} - \frac{T_L}{m_\chi} f_{10}. \end{aligned} \quad (36)$$

The effective sound speed squared of the CDM fluid is

$$c_\chi^2 = \frac{T_\chi}{m_\chi} \left(1 - \frac{1}{3} \frac{d \ln T_\chi}{d \ln a} \right), \quad (37)$$

which differs from the thermal speed squared T_L/m_χ appearing in (24). This difference arises because the Laguerre expansion uses eigenfunctions of the Fokker-Planck operator which depends on the relativistic lepton temperature T_L rather than the WIMP temperature T_χ .

After kinetic decoupling, T_χ/T_L drops and the higher-order expansion coefficients f_{nl} will increase to compensate for this difference, as we already found happening with the unperturbed distribution function in (23).

The variables in (36) describe fluctuations of an imperfect fluid. The reader may wonder how a single component fluid can have an entropy perturbation. A weakly imperfect fluid is described by an equation of state $p = p(\rho, S)$ where S is the entropy which may vary in space and time. However, the WIMP gas is more complicated because it becomes fully collisionless after kinetic decoupling; it may be regarded as a superposition of many non-interacting ideal gases.

The time evolution of the imperfect fluid variables follows from Eqs. (24) [24]:

$$\dot{\delta} + k^2 u = 3\dot{\Psi}, \quad (38a)$$

$$\dot{u} + \mathcal{H}u = \Phi + c_\chi^2 \delta + \sigma - k^2 \pi - \gamma a(u - u_L), \quad (38b)$$

$$\begin{aligned} \dot{\sigma} + 2\mathcal{H}\sigma + \left(\frac{5}{3}\frac{T_L}{m_\chi} - c_\chi^2\right)k^2 u - \frac{5}{4}\left(\frac{2T_L}{m_\chi}\right)^{3/2}k f_{11} \\ = -\frac{1}{a^2}\frac{d}{d\tau}(a^2 c_\chi^2)\delta + 3\dot{\Psi}\left(\frac{5}{3}\frac{T_\chi}{m_\chi} - c_\chi^2\right) \\ - 2\gamma a\left[\sigma - \frac{T_1}{m_\chi} - \left(\frac{T_L}{m_\chi} - c_\chi^2\right)\delta\right], \end{aligned} \quad (38c)$$

$$\begin{aligned} \dot{\pi} + 2\mathcal{H}\pi = \frac{4}{3}\frac{T_L}{m_\chi}u - \left(\frac{2T_L}{m_\chi}\right)^{3/2}\left(\frac{21}{4}\frac{f_{03}}{k} + \frac{f_{11}}{k}\right) \\ - 2\gamma a\pi. \end{aligned} \quad (38d)$$

These equations are similar to those of an imperfect gas coupled to the lepton fluid. However, they differ significantly from the Navier-Stokes equations assumed in Ref. [4]. In place of a bulk viscosity term $\zeta k^2 u$ and a shear viscosity term $\frac{4}{3}\eta k^2 u$ where ζ and η are the bulk and shear viscosity coefficients (divided by the mass density), (38b) has an entropy term σ and a shear stress term $-k^2 \pi$ where σ and π are not proportional to u . The usual Chapman-Enskog expansion does not apply to our Fokker-Planck equation when the collision mean-free path becomes large. Moreover, because of the f_{11} and f_{03} terms, Eqs. (38) do not form a closed system. Nonetheless, these equations are useful for providing insight and they will guide us to a very good approximation to the full numerical solution of the Fokker-Planck equation.

Prior to kinetic decoupling, when the damping terms proportional to γa are large, the solutions to (38) have $\delta = \delta_L$, $u = u_L$, $\sigma = \pi = 0$, in agreement with (27). Entropy and shear stress perturbations develop during decoupling as the CDM gas becomes collisionless. These in turn modify and damp the acoustic oscillations of the gas.

It is instructive to solve the imperfect fluid equations with several different approximations, in order to deduce which physical effects are responsible for the features of the transfer functions shown in Fig. 1. The most extreme approximation is to completely neglect the CDM temperature and coupling to other particles, so as to describe a

perfect cold, collisionless gas. This approximation consists of setting $c_\chi^2 = \sigma = \pi = \gamma = 0$ retaining only the gravitational interaction between the CDM and the relativistic plasma. In this case the exact solution prior to neutrino decoupling for isentropic initial conditions is

$$\begin{aligned} \frac{\nu}{9} &= \frac{\cos\theta + \theta\sin\theta}{\theta^2} - \text{Ci}(\theta) + \ln\theta - \frac{1}{\theta^2} + \mathcal{C} - \frac{1}{2}, \\ \mathcal{H}u &= \frac{3}{\theta^3}(\sin\theta - \theta), \end{aligned} \quad (39)$$

where $\theta = k\tau/\sqrt{3}$, $\mathcal{C} = 0.5772\cdots$ is the Euler-Mascheroni constant, and $\text{Ci}(\theta)$ is the cosine integral. This solution is shown by the monotonically increasing curve in Fig. 1. We see that once the wavelength becomes smaller than the relativistic acoustic horizon and the potentials oscillate faster than the CDM can respond, the CDM density perturbation growth slows to logarithmic in time. This suppression is responsible for the turnover of the low-redshift CDM power spectrum from $P(k) \propto k$ at long wavelengths to $P(k) \propto k^{-3} \ln^2(k)$ at short wavelengths. However, the approximation of a cold, collisionless fluid includes none of the physical effects of kinetic decoupling.

The next simplest approximation is to treat the CDM as being cold ($c_\chi^2 = \sigma = \pi = 0$) but to include the friction term $-\gamma a(u - u_L)$ in the velocity equation. This approximation is exact in the limit $T_d/m_\chi \rightarrow 0$ hence it reproduces the case $T_d/m_\chi = 0$ in Fig. 1. We can find the solution in the limit $\tau \gg \tau_d$ by first noting that the general solution of the second-order system $\dot{\delta} + k^2 u = 3\dot{\Psi}$, $\dot{u} + \mathcal{H}u = \Phi$ is given by

$$\begin{aligned} \frac{\nu}{9} &= \frac{\cos\theta + \theta\sin\theta}{\theta^2} - \text{Ci}(\theta) + f_1\left(\ln\theta - \frac{1}{\theta^2}\right) + f_2, \\ \mathcal{H}u &= \frac{3}{\theta^3}(\sin\theta - f_1\theta), \end{aligned} \quad (40)$$

where f_1 and f_2 are independent of τ but may depend on k . Including the damping terms in (38b) promotes f_1 and f_2 to functions $f_1(k, \tau)$ and $f_2(k, \tau)$ obeying the differential equations

$$\dot{f}_1 + \gamma a f_1 = \gamma \left(\cos\theta + \frac{1}{2}\theta\sin\theta\right), \quad (41a)$$

$$\dot{f}_2 + \dot{f}_1 \ln\theta = 0. \quad (41b)$$

In the strongly-coupled limit $\tau \ll \tau_d$ the solution must match Eqs. (26), which gives

$$\begin{aligned} f_1(k, \tau) &\rightarrow \cos\theta + \frac{1}{2}\theta\sin\theta, \\ f_2(k, \tau) &\rightarrow \text{Ci}(\theta) - \left(\cos\theta + \frac{1}{2}\theta\sin\theta\right)\ln\theta \\ &\quad - \frac{1}{2}\cos\theta. \end{aligned} \quad (42)$$

The exact solution of (41) satisfying these initial condi-

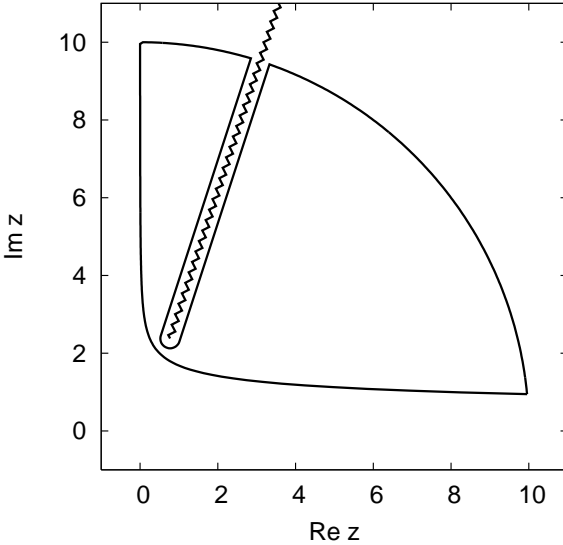


FIG. 2: Contour used to evaluate the integral in Eq. (44). The quarter-circle is actually taken to have a much larger radius than shown so that its contributions to the contour integral vanish. The desired path for the integral is along the lower left curve that joins the quarter-circle.

x	f_{res}								
0.0	1.0000	1.0	-0.1637	2.0	0.0252	3.0	0.0099	4.0	-0.0101
0.1	0.5744	1.1	-0.1562	2.1	0.0345	3.1	0.0039	4.1	-0.0082
0.2	0.3791	1.2	-0.1409	2.2	0.0403	3.2	-0.0013	4.2	-0.0062
0.3	0.2275	1.3	-0.1202	2.3	0.0427	3.3	-0.0056	4.3	-0.0042
0.4	0.1063	1.4	-0.0965	2.4	0.0424	3.4	-0.0090	4.4	-0.0022
0.5	0.0109	1.5	-0.0716	2.5	0.0397	3.5	-0.0113	4.5	-0.0004
0.6	-0.0610	1.6	-0.0471	2.6	0.0352	3.6	-0.0126	4.6	0.0011
0.7	-0.1196	1.7	-0.0244	2.7	0.0295	3.7	-0.0130	4.7	0.0023
0.8	-0.1443	1.8	-0.0045	2.8	0.0231	3.8	-0.0126	4.8	0.0033
0.9	-0.1606	1.9	0.0122	2.9	0.0164	3.9	-0.0116	4.9	0.0039

TABLE I: Residuals from the steepest descent approximation to $f_1(x)$, defined in Eqs. (44) and (45).

tions is given by a pair of quadratures,

$$\begin{aligned}
 f_1(k, \tau) &= \int_0^\tau e^{(s-s')/2} \left(\cos \theta' + \frac{1}{2} \theta' \sin \theta' \right) \gamma' a' d\tau' , \\
 f_2(k, \tau) &= \int_0^\tau [f_1(k, \tau') - 1] \frac{d\tau'}{\tau'} + (1 - f_1) \ln \theta \\
 &\quad + \mathcal{C} - \frac{1}{2} ,
 \end{aligned} \tag{43}$$

where $s \equiv \frac{1}{2} \gamma a \tau = (\tau/\tau_d)^{-4}$, $\theta \equiv k\tau/\sqrt{3}$, and primed quantities are evaluated at τ' .

The late-time solution is dominated by f_1 , which for

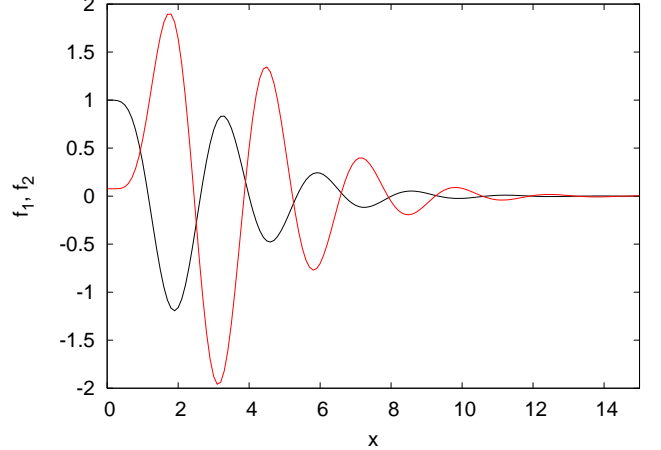


FIG. 3: The auxiliary functions $f_1(x)$ and $f_2(x)$ (the curve with the higher amplitude of oscillation) appearing in Eq. (40), where $\tau \gg \tau_d$ and $x \equiv (k\tau_d/2\sqrt{3})^{4/5}$.

$\tau \gg \tau_d$ becomes the following function of wavenumber,

$$f_1(x) = \mathcal{R}e \int e^{-z(r)} \frac{(1 + x r e^{-i2\pi/5})}{r^5 - 1} dz , \quad x \equiv \left(\frac{k\tau_d}{2\sqrt{3}} \right)^{4/5} . \tag{44}$$

The complex function $z(r) = x e^{-i2\pi/5} (\frac{1}{2} r^{-4} + 2r)$ where r itself is complex but cannot be used as the integration variable because of the essential singularity at $r = 0$. The contour used to evaluate f_1 is shown in Fig. 2. Using the steepest descent approximation to evaluate the contributions along the branch cut gives

$$\begin{aligned}
 f_1(x) &= \left(\frac{4\pi x}{5} \right)^{1/2} \exp \left[-\frac{5}{2} x \cos \left(\frac{2\pi}{5} \right) \right] \\
 &\quad \times \left[\cos \left(\varphi - \frac{\pi}{5} \right) + x \cos \left(\varphi - \frac{3\pi}{5} \right) \right] + f_{\text{res}}(x) , \\
 \varphi &\equiv \frac{5x}{2} \sin \left(\frac{2\pi}{5} \right) ,
 \end{aligned} \tag{45}$$

where $f_{\text{res}}(x)$ is a correction to the steepest descent approximation, evaluated numerically and tabulated for interpolation in Table I. For $x \ll 1$, $1 - f_1$ goes to zero faster than x^4 , with $f_1(0.2) = 0.9990$.

Numerical integration yields an approximate fit to $f_2(x)$ for $x \gg 1$ similar to (45):

$$f_2(x) \approx -3.45 x^{0.75} \exp \left[-\frac{5}{2} x \cos \left(\frac{2\pi}{5} \right) \right] (x \sin \varphi - \cos \varphi) , \tag{46}$$

Figure 3 shows the results for $f_1(x)$ and $f_2(x)$. Although f_2 has larger amplitude, f_1 dominates the contribution to the CDM transfer function for $\tau \gg \tau_d$.

This calculation shows that, in the limit of large WIMP mass $m_\chi \gg T_d$, the free-streaming suppression of the

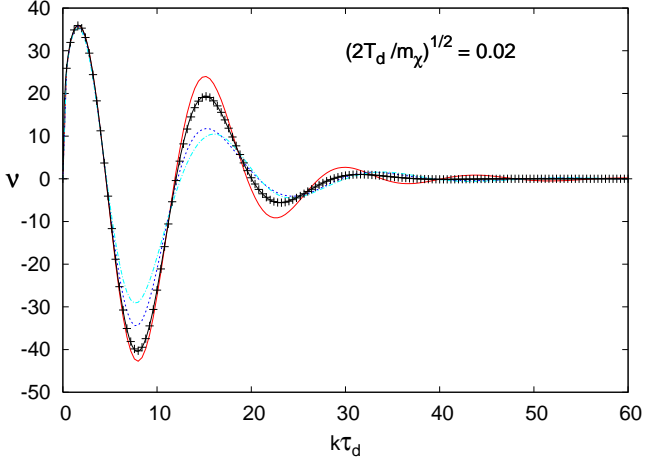


FIG. 4: CDM transfer function and several approximations plotted versus wavenumber at conformal time $\tau = 72\tau_d$. In descending amplitude of the second peak, the curves are (1) fluid approximation with $\pi = \sigma = 0$, (2) exact solution of the Fokker-Planck equation, (3) imperfect fluid approximation with shear stress but no entropy perturbation; (4) imperfect fluid approximation with both shear stress and entropy perturbations. The plus signs superimposed on the exact solution curve are the solution with $T_d/m_\chi = 0$, multiplied by a Gaussian damping factor as described in the text.

transfer function is not Gaussian but instead is exponential in $x \propto k^{4/5}$.

Allowing a nonzero T_d/m_χ introduces a Gaussian suppression, as follows. Including the $c_\chi^2 \delta$ term in (38b) adds the term $-k^2 c_\chi^2 \tau \nu/9$ to the right-hand side of (41a). With the leading late-time behavior $\epsilon/9 \approx f_1 \ln \theta$, this gives an approximate Gaussian suppression,

$$\nu(k, \tau) \approx \exp\left(-\frac{1}{2} \frac{k^2}{k_s^2}\right) \nu_0(k, \tau), \quad k_s^{-1} \equiv \int_0^\tau c_\chi(\tau') d\tau', \quad (47)$$

where $\nu_0(k, \tau)$ is the solution for $T_d/m_\chi = 0$ given by (40) and (43). While (47) is similar to (32) and (33), the Gaussian cutoff distance differs from the free-streaming distance (34) by a factor $\sqrt{5/3}$.

Equations (40) and (47) assume that the CDM behaves like a perfect fluid [25]. By integrating (38) numerically with the simplification $f_{11} = f_{03} = 0$, we can include effects of nonzero shear stress π and entropy perturbation σ . The results are shown in Fig. 4 in comparison with the exact solution from Fig. 1. While the effects of nonzero temperature, shear stress, and entropy perturbations qualitatively reproduce the suppression of the transfer function, none of the fluid approximations gives a good match to the exact solution of the Fokker-Planck equation. However, an excellent fit (with maximum error about one percent of the oscillation amplitude) is given

by a modification of (47),

$$\nu(k, \tau) \approx \exp\left(-\frac{1}{2} \frac{k^2}{k_{fs}^2}\right) \nu_0(k, \tau),$$

$$k_{fs}^{-1} \equiv \sqrt{\frac{6T_d}{5m_\chi}} \int_{\tau_*}^\tau \frac{d\tau}{a/a_d}. \quad (48)$$

This approximation, with $\tau_* = 1.05\tau_d$, is shown by the plus signs in Fig. 4. The coefficient in front of the integral defining k_{fs}^{-1} was found numerically; the value $\frac{6}{5} = 1.200$ is numerically correct to 0.1% or better and clearly differs from the coefficient $\Gamma(\frac{3}{4}) = 1.2254\cdots$ appearing in the free-streaming prediction of (34) as well as the perfect fluid prediction $\frac{5}{3}\Gamma(\frac{4}{3}) = 2.0423\cdots$ of (47).

The modified form of thermal damping suggests that on small scales the WIMP gas might be described as a thermal gas with ratio of specific heats $1.2/\Gamma(\frac{4}{3}) = 0.979\cdots$ instead of $\frac{5}{3}$. However, numerical tests showed that no perfect gas equation of state can reproduce the exact solution of the Fokker-Planck equation as well as (48). We will therefore use (48) to calculate the effects of free-streaming damping even though it is based on a numerical instead of an analytic solution. Note that (48) is valid through pair annihilation and radiation-matter equality because the free-streaming distance is proportional to $\int \sqrt{T_\chi/m_\chi} d\tau$ and $T_\chi \propto (a/a_d)^{-2}$ at all times after WIMP decoupling.

The physics of WIMP decoupling is similar but not identical to the much later decoupling of atoms at a temperature of 0.25 eV. In both cases the decoupled particles bear the imprint of acoustic oscillations while they were coupled to a relativistic gas. In both cases the acoustic oscillations are damped by friction during decoupling (Silk damping), although the damping is exponential in $k^{4/5}$ for WIMPs as opposed to k^2 for atoms. In both cases short-wavelength fluctuations are damped further by thermal motions after decoupling. However, the last stage differs for the two gases because the atomic gas remains collisional (hence damping takes place for wavelengths shorter than the Jeans length) while the CDM gas is collisionless and the relevant scale is the free-streaming length. As a result the CDM gas develops shear stress and entropy perturbations in (38b) that are not present for a collisional gas. Nonetheless these perturbations lead to free-streaming damping that is qualitatively similar to the Jeans damping of a collisional gas.

The physics of perturbation evolution can be simpler to interpret in position space than in Fourier space [13]. Figure 5 shows the one-dimensional Green's function defined by

$$\nu^{(1)}(x, \tau) = \frac{1}{2\pi} \int_{-\infty}^{\infty} e^{i\mathbf{k}\cdot\mathbf{x}} \nu(k, \tau) dk. \quad (49)$$

In real space the Green's function is essentially a wave packet of sound that started at $x = 0$ and propagated until kinetic decoupling after which time it froze in place. The oscillations in k -space arise solely because the wave

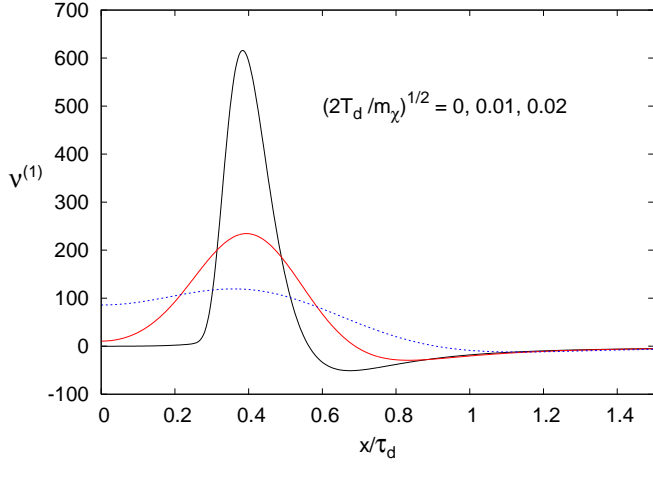


FIG. 5: Real space CDM Green's function (Fourier transform of the transfer function) at conformal time $\tau = 10^7 \tau_d$, approximately at the end of the radiation-dominated era. An initial planar perturbation sends an acoustic wave through the relativistic plasma. This wave travels through the CDM until kinetic decoupling ends; thereafter the wave is frozen in place but grows logarithmically in amplitude. The three curves show the effect of diffusion with increasing CDM temperature.

packet in real space has a rapid change in slope at its trailing edge. In the absence of WIMP-lepton coupling, $\nu^{(1)}$ would have a delta function singularity at $x = 0$ and a compensating underdense tail at $x > 0$ due to the gravitational perturbation caused by the outgoing acoustic wave in the relativistic plasma [13].

Until now we have assumed that the photon-lepton plasma is a perfect relativistic gas with $p = \frac{1}{3}\rho$. This approximation breaks down after neutrino decoupling and during electron/positron pair annihilation. The effects of neutrino free-streaming are small and are already included in numerical codes such as CMBFAST and COSMICS but pair annihilation is not. As we show next, pair annihilation also results in a minor modification of the CDM transfer function on small scales.

IV. EVOLUTION THROUGH PAIR ANNIHILATION

During electron-positron annihilation the equation of state changes slightly, modifying the evolution of perturbations. Neglecting the small amount of neutrino heating that takes place during pair annihilation, after CDM kinetic decoupling the energy density and pressure of the

photons, 3 flavors of neutrinos, and electron pairs is

$$\begin{aligned} \rho_\gamma &= 3p_\gamma = \frac{\pi^2 T_\gamma^4}{15}, & \rho_\nu &= 3p_\nu = \frac{7\pi^2 T_\nu^4}{40a^4}, \\ \rho_\pm &= \frac{2T_\gamma^4}{\pi^2} R(\xi), & p_\pm &= \frac{2T_\gamma^4}{3\pi^2} P(\xi), \end{aligned} \quad (50)$$

where $\xi \equiv m_e/T_\gamma$ and $T_{\nu 0} \equiv aT_\nu = \text{constant}$. The pair density and pressure are given in terms of the Fermi-Dirac integrals

$$\begin{aligned} R(\xi) &\equiv \int_0^\infty \frac{x^2 \sqrt{x^2 + \xi^2} dx}{e^{\sqrt{x^2 + \xi^2}} + 1}, \\ P(\xi) &\equiv \int_0^\infty \frac{x^4 dx}{\sqrt{x^2 + \xi^2} (e^{\sqrt{x^2 + \xi^2}} + 1)}. \end{aligned} \quad (51)$$

Energy conservation for the photon-pair plasma gives

$$\frac{d \ln \xi}{d \ln a} = \frac{A}{B}, \quad (52)$$

where

$$\begin{aligned} A &\equiv 1 + \frac{30R}{\pi^4} + \frac{15}{2\pi^4}(P - R), \\ B &\equiv 1 + \frac{30R}{\pi^4} - \frac{15}{2\pi^4} \frac{dR}{d \ln y}. \end{aligned} \quad (53)$$

The photon-pair plasma has equation of state parameter

$$w = \frac{1}{3} + \frac{(10/\pi^4)(P - R)}{1 + (30/\pi^4)R + (21/8)(T_\nu/T_\gamma)^4} \quad (54)$$

and sound speed squared

$$3c_w^2 = 1 + \frac{A(A - B)}{B[A + (21/8)(T_\nu/T_\gamma)^4]}. \quad (55)$$

These are plotted in Fig. 6. Pair annihilation makes a 10% dip in the equation of state.

The relation between expansion factor and conformal time follows from integrating the Friedmann equation

$$\dot{a}^2 = \frac{4\pi^3 G(aT_\gamma)^4}{45} g_{\text{eff}}, \quad (56)$$

where

$$g_{\text{eff}} = \frac{30}{\pi^2} \left(\frac{\rho_\gamma + \rho_\nu + \rho_\pm}{T_\gamma^4} \right) = 2 + \frac{21}{4} \left(\frac{T_\nu}{T_\gamma} \right)^4 + \frac{60}{\pi^4} R. \quad (57)$$

Neglecting the small neutrino shear stress arising from free-streaming after neutrino decoupling at $T \sim 2$ MeV, the conformal Newtonian gauge gravitational potentials $\Phi = \Psi$ obey the evolution equation

$$\ddot{\Phi} + 3(1 + c_w^2)\mathcal{H}\dot{\Phi} + 3(c_w^2 - w)\mathcal{H}^2\Phi + k^2 c_w^2 \Phi = 0. \quad (58)$$

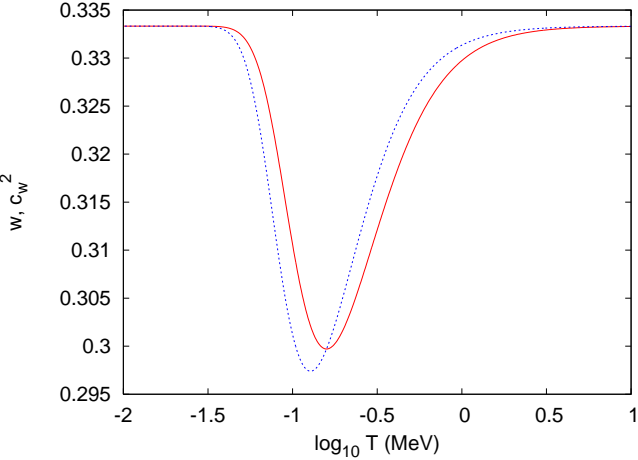


FIG. 6: Equation of state parameter w (solid curve) and effective sound speed squared c_w^2 (dotted curve) through the period of electron pair annihilation.

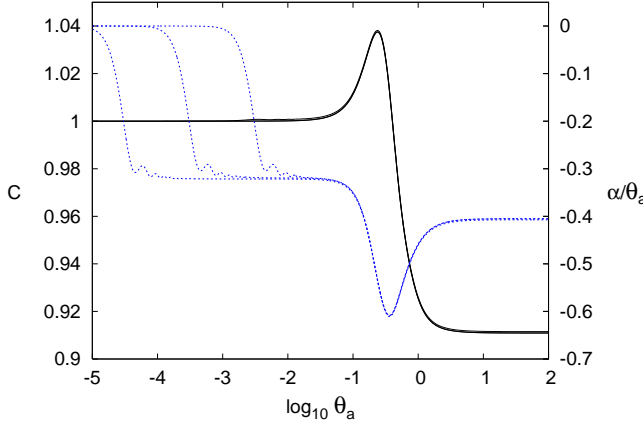


FIG. 7: Amplitude C (solid curve) and phase shift α (dashed curves, normalized by $\theta_a = k\tau_a/\sqrt{3}$) for the gravitational potential Ψ of Eq. (59), for $\tau \gg \tau_a$, plotted versus θ_a (dimensionless wavenumber). Three sets of curves are shown, corresponding to the times $\tau = (10^3, 10^4, 10^5) \tau_a$. Before pair annihilation, $C = 1$ and $\alpha = 0$ for all k .

Long after pair annihilation is completed, $w = c_w^2 = \frac{1}{3}$ and the solution is

$$\Phi(k, \tau) = -\frac{3C}{\theta^3} [\sin(\theta + \alpha) - \theta \cos(\theta + \alpha)] , \quad (59)$$

where C (not to be confused with the collisional coupling constant of Eq. 3) and α are independent of τ but may depend on k . Before pair annihilation, $C = 1$ and $\alpha = 0$. During pair annihilation, C and α change but after pair annihilation they become independent of time.

We define a characteristic conformal time for pair an-

nihilation, τ_a , by scaling from the decoupling time:

$$\tau_a \equiv \tau_d \left(\frac{T_d}{0.511 \text{ MeV}} \right) . \quad (60)$$

Pair annihilation imprints features on $\Phi(k, \tau)$ at wavenumbers $k \sim \tau_a^{-1}$. After pair annihilation is completed, we expect C and α in (59) to depend only on $k\tau_a$. Numerical integration of (58) yields the results shown in Fig. 7. Pair annihilation leads to a small change in the amplitude C of gravo-acoustic oscillations and a characteristic phase shift α of order $\theta_a \equiv k\tau_a/\sqrt{3}$. Wavelengths much longer than the acoustic horizon length ($\theta = k\tau/\sqrt{3} \ll 1$) are unmodified. Waves that enter the Hubble length when the effective sound speed is reduced by pair annihilation (Fig. 6) are amplified because with decreasing sound speed, pressure forces are less able to prevent gravitational growth. The diminished sound speed also changes the distance traveled by acoustic waves, leading to a phase shift for wavelengths smaller than the acoustic horizon distance. The propagation of the acoustic horizon is evident in the propagating steps in α/θ_a in Fig. 7. Although these steps would appear to prevent Φ from relaxing to (59) with time-independent C and α , for $\tau \gg \tau_a$, $\theta \gg |\theta_a|$ and one may set $\alpha = 0$ with an error in Φ of $O(\tau_a/\tau)$. Wavelengths much longer than the Hubble length during pair annihilation are essentially unmodified.

Still shorter waves are described by the WKB solution of (58),

$$\Phi(k, \tau) \propto \left(\frac{\rho + p}{c_w} \right)^{1/2} \cos \int_0^\tau k c'_w d\tau' \quad \text{for } k\tau \gg 1 . \quad (61)$$

The dip in the sound speed during pair annihilation leads to a phase shift $\alpha = k \int_0^\tau (c'_w - 1/\sqrt{3}) d\tau' = -0.405\theta_a$ for $\theta_a \gg 1$ and $\tau \gg \tau_a$. Pair annihilation effectively resets the starting time for acoustic oscillations from $\tau = 0$ to $\tau = 0.405\tau_a$.

Similarly the change in energy density and pressure through pair annihilation leads to a change in amplitude. In the WKB approximation, one finds that for $k\tau_a \gg 1$ the amplitude C of $\Phi(k, \tau)$ changes through pair annihilation by a factor

$$C(k) \rightarrow \frac{\dot{a}(\tau_1)}{\dot{a}(\tau_2)} = \left(\frac{T_\nu}{T_\gamma} \right)_{\tau_2}^{1/2} \left[\frac{g_{\text{eff}}(\tau_1)}{g_{\text{eff}}(\tau_2)} \right]^{1/2} = 0.911 , \quad (62)$$

where $\tau_1 \ll \tau_a \ll \tau_2$. The WKB results for $\alpha(k)$ and $C(k)$ match the numerical results shown in Fig. 7.

The change in the gravitational potential caused by pair annihilation induces changes in the CDM growth. The late-time solution of (38a)–(38b) with $T/m_\chi = 0$ is

$$\begin{aligned} \frac{\nu_0}{9C} &= \frac{\cos \tilde{\theta} + \theta \sin \tilde{\theta}}{\theta^2} - \cos \alpha \text{Ci}(\theta) + \sin \alpha \text{Si}(\theta) \\ &\quad + f_3 \left(\ln \theta - \frac{1}{\theta^2} \right) + f_4 , \\ \mathcal{H}u_0 &= \frac{3C}{\theta^3} [\sin \tilde{\theta} - f_3 \theta] , \end{aligned} \quad (63)$$

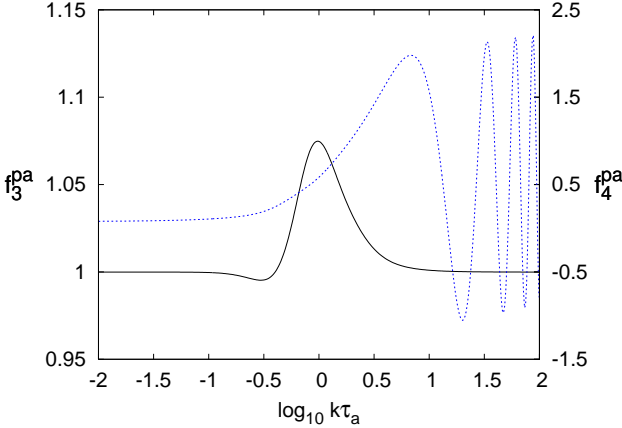


FIG. 8: Amplitude functions f_3^{pa} (solid curve) and f_4^{pa} (dashed curve) for the gravitational CDM density perturbation ν of Eq. (63), for $\tau \gg \tau_a$, plotted versus wavenumber. For $k\tau_a \ll 1$, $f_3^{\text{pa}} = 1$ and $f_4^{\text{pa}} = \mathcal{C} - \frac{1}{2} = 0.0772 \dots$. This figure assumes that the CDM is always collisionless and was never coupled to the radiation. The results show there is a 7% enhancement of growth for waves that enter the horizon during pair annihilation.

where $\tilde{\theta} \equiv \theta + \alpha$ and the subscript 0 indicates $T/m_\chi = 0$. After pair annihilation the transfer functions f_3 and f_4 depend on k but not on τ .

Kinetic decoupling introduces a length scale τ_d . Pair annihilation introduces a second scale, τ_a . When $\tau_a \gg \tau_d$ these two physical effects can be separated. Thus we consider first the case of purely collisionless CDM, i.e. $\gamma = 0$ in (38), in which case there is no kinetic decoupling. Now there is only one timescale in the problem, τ_a , and we denote the corresponding transfer functions in (63) by f_3^{pa} and f_4^{pa} . The results obtained by numerical integration are shown in Fig. 8. For $k\tau_a \ll 1$, $f_3^{\text{pa}} \approx 1 - 3.00(k\tau_a)^4$ (where the coefficient 3.00 was found by numerical integration) and $f_4^{\text{pa}} \approx \mathcal{C} - \frac{1}{2}$. For $k\tau_a \gg 1$, the WKB approximation yields

$$\begin{aligned} f_3^{\text{pa}} &\approx 1 - 0.1067(k\tau_a)^{-2}, \\ f_4^{\text{pa}} &\rightarrow -\frac{\pi}{2} \sin \alpha + \left[\frac{1}{C(k)} - 1 \right] \ln(9.82k\tau_a), \end{aligned} \quad (64)$$

where the coefficients 0.1067 and 9.82 were determined by numerical integration. The errors made by assuming (64) are less than 1% for $k\tau_a > 100$.

For WIMP dark matter, the effects of kinetic decoupling and pair annihilation combine to give transfer functions $f_3^{\text{kd+pa}}$ and $f_4^{\text{kd+pa}}$ in (63). For $T/m_\chi = 0$ and $\tau_d \ll \tau_a \ll \tau$ these are

$$\begin{aligned} f_3^{\text{kd+pa}}(k) &= f_1(k)f_3^{\text{pa}}(k), \\ f_4^{\text{kd+pa}}(k) &= f_4^{\text{pa}}(k) + \frac{1}{C(k)} \left[f_2(k) - \mathcal{C} + \frac{1}{2} \right] \\ &+ [f_1(k) - 1] \left\{ \left[\frac{1}{C(k)} - 1 \right] \ln(1.589k\tau_a) - \ln C(k) \right\}. \end{aligned} \quad (65)$$

The coefficient 1.589 was found numerically but otherwise $f_3^{\text{kd+pa}}$ and $f_4^{\text{kd+pa}}$ were determined analytically. The general transfer function is given in terms of separate transfer functions for kinetic decoupling (f_1, f_2) and pair annihilation ($f_3^{\text{pa}}, f_4^{\text{pa}}$).

Pair annihilation modifies the CDM velocity and density transfer functions at $k \sim \tau_a^{-1}$ due to the peak in $f_3^{\text{pa}}(k)$. There is also a small modification of the density for $k\tau_a \gg 1$. In the limit $k\tau \gg k\tau_a \gg 1$,

$$\frac{\nu_0}{9} \rightarrow f_1(k) \left[\ln \theta + 0.08909 \ln \left(\frac{7.416\tau_a}{\tau} \right) \right] + f_2(k). \quad (66)$$

Comparing this with (40), we see that the term proportional to $1 - C(\infty) = 0.08909$ is induced by pair annihilation. This effect arises from the reduction of the gravitational potential by a factor $C(\infty) = \dot{a}(\tau_1)/\dot{a}(\tau_2)$ at short wavelengths after pair annihilation. However, the correction to ν is always less than 9%.

The full density transfer function for nonzero CDM temperature during the radiation-dominated era follows from (48), (63), and (65). Numerical tables of the transfer functions $f_1(k\tau_d)$, $f_2(k\tau_d)$, $C(k\tau_a)$, $\alpha(k\tau_a)$, $f_3^{\text{pa}}(k\tau_a)$, and $f_4^{\text{pa}}(k\tau_a)$ are available from the author.

V. EVOLUTION THROUGH RADIATION-MATTER EQUALITY

Following kinetic decoupling and pair annihilation there is one additional major life event for CDM density fluctuations before they collapse to form nonlinear structures: the transition to a matter-dominated universe occurring at $1+z_{\text{eq}} \equiv a_{\text{eq}}^{-1} \approx 3200$. The constituents include photons, neutrinos, baryons, and CDM. The background equation of state is modified by the presence of nonrelativistic baryons and CDM,

$$3w = \frac{1}{1+y}, \quad y = \frac{\rho_b + \rho_c}{(g_{\text{eff}}/2)\rho_\gamma} = \frac{a}{a_{\text{eq}}}. \quad (67)$$

Assuming that dark energy and spatial curvature can be neglected during the times of interest, the solution of the Friedmann equation for $\tau \gg \tau_a$ is

$$\sqrt{1+y} = 1 + \frac{\tau}{2\tau_e}, \quad \tau_e \equiv \sqrt{\frac{a_{\text{eq}}}{\Omega_m H_0^2}}. \quad (68)$$

Here Ω_m is the present-day density parameter for $\rho_m \equiv \rho_b + \rho_c$.

Before recombination, Thomson scattering couples the photons and baryons so that they behave as a single fluid with sound speed given by

$$3c_{\gamma b}^2 = \left(1 + \frac{3}{4} \frac{\rho_b}{\rho_\gamma} \right)^{-1}. \quad (69)$$

We make two approximations which enable us to reduce the dynamics to a fourth-order system in time, for

which we obtain limiting analytic solutions: Photons and baryons behave like a single perfect fluid and neutrino shear stress is neglected. (We also assume a flat background, $K = 0$, but this is always a good approximation during the times of interest.) These approximations introduce small errors in the results which may be eliminated by integrating the full system of equations for photons, neutrinos, baryons, and CDM with CMBFAST [12] or equivalent starting after pair annihilation from initial conditions obtained in the preceding section. However, the simplified dynamics leads to analytic results making it easy to distinguish the various physical effects in the transfer functions.

With these assumptions and the further restrictions $\tau \gg \tau_a$ and $T_d/m_\chi \ll 1$, the perturbed Einstein equations may be combined to yield an equation of motion for the gravitational potential $\Phi = \Psi$,

$$\ddot{\Phi} + 3(1 + c_{\gamma b}^2)\mathcal{H}\dot{\Phi} + 3(c_{\gamma b}^2 - w)\mathcal{H}^2\Phi + k^2c_{\gamma b}^2\Phi = -A_c c_{\gamma b}^2 \left(\delta_c - \frac{\rho_b \rho_\nu}{\rho_c \rho_\gamma} \delta_\nu \right), \quad (70)$$

where δ_c and δ_ν are, respectively, the CDM and neutrino density perturbation in conformal Newtonian gauge, and we have defined

$$A_c \equiv 4\pi G a^2 \rho_c = \frac{3}{2} \frac{(1 - f_b)y}{1 + y} \mathcal{H}^2, \quad (71)$$

where $f_b \equiv \Omega_b/\Omega_m$. Equation (70) is a modified form of (58). The CDM fluid equations (38) remain valid with $\delta = \delta_c$, $u = u_c$.

The evolution of metric perturbations is coupled to the evolution of both CDM and neutrino perturbations. To simplify the presentation we avoid solving the collisionless Boltzmann equation for neutrinos. Instead we make an additional approximation for the neutrino dynamics: either the neutrino fluid evolves like the photon-baryon fluid, or neutrino perturbations are damped by Hubble expansion on sub-horizon scales in a manner consistent with their evolution on super-horizon scales. In the first case we set $\delta_\nu = \delta_\gamma$ on all scales, which is equivalent to setting $\delta_\nu = 0$ in Eq. (70) and replacing $c_{\gamma b}$ with c_{rb} defined by

$$3c_{rb}^2 = \left[1 + \frac{3}{4} \frac{\rho_b}{(g_{\text{eff}}/2)\rho_\gamma} \right]^{-1} = \left(1 + \frac{3}{4} f_b y \right)^{-1}. \quad (72)$$

In the second case, we note that on scales much larger than the Hubble length, for isentropic (curvature) perturbations all species have the same number density perturbation, $\delta_c = \delta_\nu = \delta_\gamma$. The evolution of isentropic perturbations on large scales follows from Ref. [14]:

$$\delta_\nu \approx - \left(\frac{2}{1 + w} \right) (\Phi + \mathcal{H}^{-1}\dot{\Phi}). \quad (73)$$

On scales much smaller than the Hubble (or neutrino free-streaming) length, during the radiation-dominated

era δ_ν undergoes damped oscillations while the amplitude of the photon-baryon oscillations is constant. This qualitative behavior is correctly reproduced if one applies (73) to the neutrinos at all times while leaving (70) unchanged.

Thus, our two approximations for neutrino evolution correspond to two different choices for the sound-speed of the photon-baryon gas: either the sound speed is set to c_{rb} with $\delta_\nu = 0$ or the sound speed is $c_{\gamma b}$ with δ_ν given by (73). Either way, when the CDM dynamics is added, the evolution reduces to a fourth-order system in time. The difference between the two treatments gives a measure of the importance of massless neutrinos for CDM evolution.

Setting $\delta_\nu = 0$ and writing the sound speed as c_b which may be set to either $c_{\gamma b}$ or c_{rb} , differentiating (70) and using the CDM continuity equation gives

$$\partial_t^3 \Phi + 5\mathcal{H}\ddot{\Phi} + \frac{3}{2}\mathcal{H}^2\dot{\Phi}[3 - 5w - 3c_b^2(1 + w)] + 3A_c c_b^2 \dot{\Phi} + k^2 c_b^2 (\dot{\Phi} + \mathcal{H}\Phi) = A_c k^2 c_b^2 u_c. \quad (74)$$

Differentiating this again and using the velocity equation $\dot{u}_c + \mathcal{H}u_c = \Phi$ gives

$$\begin{aligned} \partial_t^4 \Phi + (8 - 3c_b^2)\mathcal{H}\partial_t^3 \Phi + & \left[17 - 15(w + c_b^2) - \frac{6wc_b^2}{c_{rb}^2} \right] \mathcal{H}^2 \ddot{\Phi} \\ & + \frac{9}{2} \left[(2 - 3c_b^2)(1 - 3w) + \frac{4w}{3} \left(1 - \frac{c_b^2}{c_{rb}^2} \right) \right] \mathcal{H}^3 \dot{\Phi} \\ & + k^2 c_b^2 \left[\ddot{\Phi} + 3\mathcal{H}\dot{\Phi} + \left(\frac{2}{c_{rb}^2} - 3 \right) w \mathcal{H}^2 \Phi \right] = 0. \end{aligned} \quad (75)$$

For wavelengths longer than the Hubble length this equation is correct if $c_b = c_{rb}$; for wavelengths much shorter than the Hubble length it is approximately correct if $c_b = c_{\gamma b}$. We now present the analytic solution to the fourth-order system in these two limits.

In the long-wavelength limit $k^2 \ll \mathcal{H}^2$, the four linearly independent solutions may be obtained as quadratures using the methods of Ref. [14]:

$$\Phi_1 = \frac{\mathcal{H}\tau_e}{y^2} = \frac{\sqrt{1 + y}}{y^3}, \quad (76a)$$

$$\Phi_2 = \frac{3\mathcal{H}}{2y^2} \int^\tau y^2(1 + w) d\tau, \quad (76b)$$

$$\Phi_3 = \frac{\mathcal{H}}{y^2} \int^\tau y^3 w d\tau, \quad (76c)$$

$$\Phi_4 = \frac{\mathcal{H}}{y^2} \int^\tau y^2 w [1 + (\rho_b/\rho_m)y] d\tau. \quad (76d)$$

These solutions give the time-dependence in the limit $k \rightarrow 0$ valid in both the radiation- and matter-dominated eras. The physical solution for isentropic curvature fluctuations is

$$\begin{aligned} \Phi_+ &= \frac{3}{2}\Phi_2 + \frac{8}{5}\Phi_1 \\ &= \frac{9}{10} \left(1 + \frac{2}{9y} - \frac{8}{9y^2} - \frac{16}{9y^3} + \frac{16\sqrt{1 + y}}{9y^3} \right) \\ &\approx 1 - \frac{1}{16}y \quad \text{for } y \ll 1. \end{aligned} \quad (77)$$

Mode 1 is the decaying mode. Modes 3 and 4 are entropy perturbations and (for $k^2 \ll \mathcal{H}^2$) are constants added to the other solutions,

$$\Phi_3 = \frac{4}{3} - 2\Phi_2, \quad \Phi_4 = -1 + \frac{5}{3}\Phi_2 + \frac{\rho_b}{\rho_m}\Phi_3. \quad (78)$$

In the opposite limit, $k^2 \gg \mathcal{H}^2$, approximate solutions to (75) may be found using the WKB method. The first-order WKB approximation gives two oscillatory solutions,

$$\Phi_{\pm} = (a^2 c_b^{3/2})^{-1} \exp \pm i k \int^{\tau} c_b d\tau, \quad (79)$$

and two non-oscillatory solutions of the equation

$$\ddot{\Phi} + 3\mathcal{H}\dot{\Phi} + \left(\frac{2}{c_{rb}^2} - 3\right) w\mathcal{H}^2\Phi = 0. \quad (80)$$

This equation is equivalent to the usual evolution equation for cold dark matter perturbations calculated assuming that the other components are unperturbed:

$$\ddot{D} + \mathcal{H}\dot{D} = A_c D, \quad D \propto \delta \propto y\Phi. \quad (81)$$

For $a(\tau)$ given by (67), the exact solutions of this equation are [8]

$$D_+(\tau) = P_{\nu}(1 + \tau/2\tau_e), \quad D_-(\tau) = Q_{\nu}(1 + \tau/2\tau_e), \\ \nu \equiv -\frac{1}{2} + \frac{1}{2}\sqrt{25 - 24f_b}, \quad (82)$$

where P_{ν} and Q_{ν} are Legendre functions of the first and second kind. Early in the radiation-dominated era they give

$$D_+ \approx 1 + \frac{\nu(\nu + 1)}{4} \frac{\tau}{\tau_e}, \quad D_- \approx \frac{1}{2} \ln \left(\frac{4\tau_e}{\tau} \right) \quad \text{for } \tau \ll \tau_e. \quad (83)$$

In the opposite limit,

$$D_+ \approx \frac{\Gamma(\nu + \frac{1}{2})}{\sqrt{\pi}\Gamma(\nu + 1)} \left(\frac{\tau}{\tau_e} \right)^{\nu} \\ \approx \left[\left(\nu + \frac{1}{2} \right) \frac{\tau}{\tau_e} D_- \right]^{-1} \quad \text{for } \tau \gg \tau_e. \quad (84)$$

By matching the solutions found here to those in the radiation-dominated era, (59) and (63), we obtain results for the gravitational potential Φ and synchronous gauge density perturbation ν (not to be confused with the index of the Legendre functions) valid through the matter-radiation transition. On large scales,

$$\Phi \approx -\Phi_+, \quad \nu \approx \frac{2(k\tau_e)^2 y^2 \Phi_+}{4 + 3y}, \quad k^2 \tau_e^2 \ll 1, \quad (85)$$

where we have chosen the normalization $\Phi = -1$ as $k\tau \rightarrow 0$. On scales shorter than the Jeans length,

$$\frac{\nu}{9Cf_3} \approx D_- + D_+ \ln \left(\frac{4k\tau_e}{\sqrt{3}} \right), \\ \Phi \approx -\frac{3C(c_b\sqrt{3})^{1/2}}{(kc_b\tau_e)^2} \frac{\cos(\theta + \alpha)}{y^2} - \frac{3(1 - f_b)\nu}{2(k\tau_e)^2 y}, \quad (86)$$

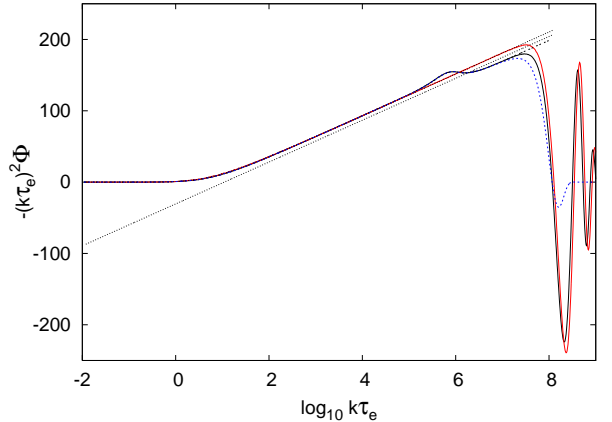


FIG. 9: Results for the gravitational potential transfer function at $y = a/a_{\text{eq}} = 10$ after the radiation-matter transition, assuming $T_d = 15.7$ MeV, $\Omega_m h^2 = 0.131$, $\Omega_b h^2 = 0.022$. The solid black curve shows the effects of pair annihilation at $T \approx 0.5$ MeV as the bump at $k\tau_e \approx 10^{5.8}$ and the effects of kinetic decoupling (with $T_d/m_{\chi} = 0$) as the damped oscillations at $k\tau_e > 10^7$; the rapidly damped dotted curve includes the effects of free-streaming damping assuming $(2T_d/m_{\chi})^{1/2} = 0.02$. Other curves show the effect of eliminating either pair annihilation or kinetic decoupling. The straight dotted line is the WKB solution of Eq. (86), vertically offset for clarity.

where $C \equiv C(k)$ and $f_3 \equiv f_3^{\text{kd+pa}}(k)$ were given in the previous section. For $k \ll \tau_a^{-1}$, $C = f_3 = 1$.

Figure 9 shows the results obtained from numerical integration of (70) using (73) to approximate the neutrino evolution. In order to illustrate the logarithmic wavenumber-dependence of the growing mode in the matter-dominated era, the potential is scaled by $-(k\tau_e)^2$ and is plotted in a semilog fashion. If instead of using (73) the neutrinos are assumed to evolve like the photon-baryon fluid, the maximal change in Φ is about 4% occurring at $k\tau_e \approx 2$ with negligible differences at much higher and lower frequencies. Thus the CDM transfer function is relatively insensitive to the detailed dynamics of massless neutrinos. For the CDM and baryon abundances used in the calculations, $D_+ = 11.34$ at $y = 10$.

The WKB result helps explain how gravitational potential fluctuations with an rms amplitude 2×10^{-5} on large scales can generate nonlinear structures at high redshift. Growth after the universe becomes matter-dominated contributes a factor $D_+ \approx 1 + \frac{3}{2}y$ once the baryons are released and join the CDM potential wells. Evolution after kinetic decoupling in the early universe contributes an additional factor $9 \ln(4k\tau_e/\sqrt{3})$. The logarithm is sometimes called the Meszaros effect [15]; it arises because acoustic oscillations in the relativistic plasma gravitationally induce velocity perturbations in the dark matter. Half of the factor of 9 (i.e., a factor of 3) arises because the comoving number density is affected by the cube of the strain $(1 - \Psi)$ in three dimensions.

Altogether, CDM density perturbations in the matter-dominated era are enhanced by a factor $\frac{27}{2}y \ln(4k\tau_e/\sqrt{3})$ which is sufficient to drive rms density perturbations nonlinear on scales below $10^{-5} M_\odot$ by a redshift of 20.

These results neglect free-streaming of the CDM particles. As shown in Section III, during the radiation-dominated era CDM free-streaming leads to a modified Gaussian suppression, Eq. (48). Including the radiation-matter transition, this gives

$$(k_{\text{fs}}\tau_d)^{-1} = \sqrt{\frac{6T_d}{5m_\chi}} \ln \left(\frac{1 + 4\tau_e/\tau_*}{1 + 4\tau_e/\tau} \right), \quad (87)$$

where $\tau_* \approx \tau_d$. For the parameters of Fig. 9 with pair annihilation, $\tau_e/\tau_d = 2.706 \times 10^7$.

VI. SMALLEST-SCALE CDM STRUCTURES

Having computed the evolution of the CDM transfer function through kinetic decoupling, pair annihilation, and radiation-matter equality, we can now make predictions for the smallest-scale CDM structures. To be definite, we adopt the standard flat Λ CDM model with $\Omega_bh^2 = 0.022$, $\Omega_ch^2 = 0.109$, $h = 0.71$, $\Omega_\Lambda = 0.740$. With these assumptions, $a_{\text{eq}}^{-1} = 3160$, $\tau_e = 147$ Mpc, $\tau_d = 5.43$ pc, and $k_{\text{fs}}^{-1} = 1.38$ pc.

The CDM density transfer function $\nu(k, \tau)$ is normalized so that the variance of $\delta\rho/\rho$ in the usual synchronous gauge is $\sigma^2 = \int \nu^2(k, \tau) P_i(k) d^3k$ where $P_i(k)$ is the spectral density of the gravitational potential Φ early in the radiation-dominated era. The radiation-era potential is related to the curvature perturbation in a flat universe $\zeta = \mathcal{R} = \kappa$ [14] by $\Phi = \frac{2}{3}\kappa$.

The treatment of this paper makes several approximations: neutrino shear stress is neglected; the Boltzmann equations for neutrinos and photons after recombination have not been integrated; and photons and baryons are assumed to be tightly coupled until $y = a/a_{\text{eq}} = 10$ ($z = 315$). To test this crude treatment of multiple fluids, we compared the resulting transfer function with that computed numerically from CMBFAST [12]. For $k\tau_e \approx 100$ (small enough so that pair annihilation and kinetic decoupling are unimportant), our $\nu(k)$ was too small by 7% (due to the delay in baryons joining CDM until $z = 315$) while for $k\tau_e < 0.1$ our $\nu(k)$ was too large by 3.6% (due to the neglect of neutrino and photon shear stress). A more accurate calculation would incorporate our transfer functions for pair annihilation and kinetic decoupling into CMBFAST or equivalent code, but this level of accuracy is unnecessary for the present purposes.

Figure 10 shows the rms mass density perturbation in a sphere containing mean mass M , which follows from

$$\sigma^2(M) = \int \nu^2(k, \tau) W^2(kR) P_i(k) d^3k, \quad (88)$$

where $W(x) = 3j_1(x)/x$ is the spherical tophat window function and $R = (3M/4\pi\rho_m)^{1/3}$. The primordial

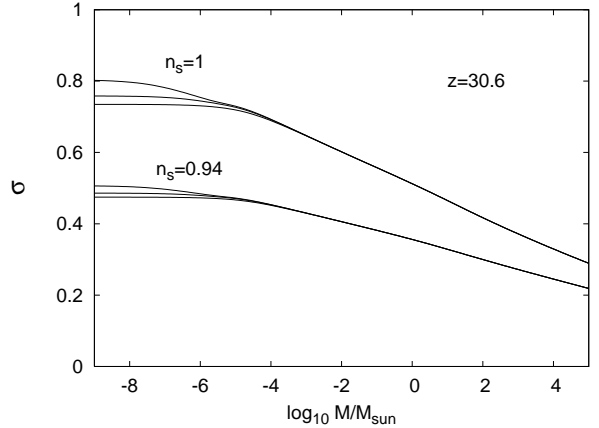


FIG. 10: RMS mass density perturbation in a sphere containing mass M , at redshift $z = 30.6$ ($a/a_{\text{eq}} = 100$). Two different assumptions are made for the scalar spectral slope n_s . For each case, three different choices are shown for the neutralino thermal speed at decoupling: $(2T_d/m_\chi)^{1/2} \in \{0, 0.01, 0.02\}$.

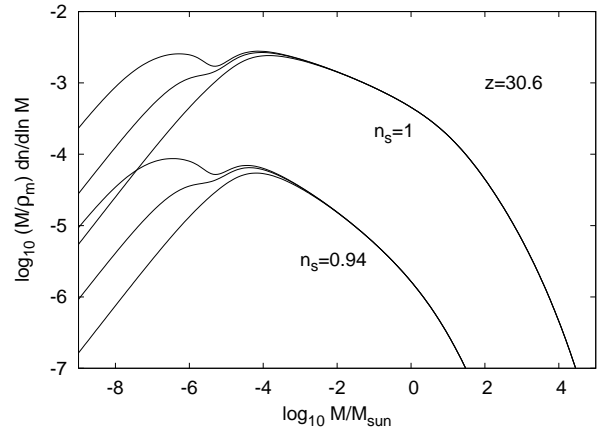


FIG. 11: Press-Schechter mass fraction for the cases shown in Fig. 10. The effects of increasing free-streaming damping are apparent in the erasure of the smallest objects with increasing $(2T_d/m_\chi)^{1/2}$. The cases of no free-streaming damping have bimodal distributions, however this requires unreasonable assumptions about the dark matter mass and couplings.

spectrum has been normalized to $\Delta_{\mathcal{R}}^2 = 2.40 \times 10^{-9}$ at $k = 0.002/\text{Mpc}$ from the WMAP 3-year results [16]. The amplitude for the scale-invariant case $n_s = 1$ is more than 50% greater than it is in the tilted model $n_s = 0.94$ favored by the data. With a neutralino mass of 100 GeV and kinetic decoupling temperature 15.7 MeV, $(2T_d/m_\chi)^{1/2} = 0.0177$. In this case, 3σ perturbations reach $\nu = 1$ by $z = 46$.

The Press-Schechter [17] mass function dn/dM obeys

$$\frac{M}{\rho_m} \frac{dn}{d\ln M} = \frac{\delta_c}{\sigma} \left(\frac{2}{\pi} \right)^{1/2} \left| \frac{d\ln \sigma}{d\ln M} \right| e^{-\delta_c^2/2\sigma^2}, \quad (89)$$

where $\delta_c = 1.686$. The results, shown in Fig. 11, suggest that the smallest CDM objects may have masses even smaller than an earth mass, $3.0 \times 10^{-6} M_\odot$.

WIMP decoupling imprints two different length scales on the spectrum: the comoving horizon size $\tau_d \propto T_d^{-1}$ and the comoving free-streaming distance $(T_d/m_\chi)^{1/2}\tau_d$; the former scale is larger and more important. The characteristic mass for the smallest objects is the CDM mass in the horizon at decoupling,

$$\begin{aligned} M_d &= \frac{4\pi}{3}\rho_m(a=1)(c\tau_d)^3 \\ &= 2.05 \times 10^{-4} \Omega_m h^2 \left(\frac{T_d \sqrt{g_{\text{eff}}}}{50 \text{ MeV}} \right)^{-3} M_\odot \\ &= 7.59 \times 10^{-3} C^{3/4} \left(\frac{m_\chi \sqrt{g_{\text{eff}}}}{100 \text{ GeV}} \right)^{-15/4} M_\odot, \quad (90) \end{aligned}$$

where C was defined in (3). With the default values $C = 0.186$ and $g_{\text{eff}} = 10.75$, $M_d = 2.47 \times 10^{-5} M_\odot$, or

$$M_d = 1.0 \times 10^{-4} \left(\frac{T_d}{10 \text{ MeV}} \right)^{-3} M_\odot, \quad (91)$$

in agreement with Ref. [9]. Berezhinsky et al. [5] derived a different characteristic mass assuming that diffusion followed by free-streaming damping sets the minimum object mass. As we have shown, for $(2T_d/m_\chi)^{1/2} \ll 1$, the dominant damping process is not diffusion or free streaming but friction between WIMPs and relativistic leptons during kinetic decoupling (Silk damping). That this is not a diffusive process may be seen by its persistence in the limit $T_d/m_\chi = 0$.

The evolution of the mass function requires computing the density perturbations at smaller redshift. The baryons present a slight complication because after recombination, even though they are free to move apart from the photon gas, they resist gravitational instabilities for $k > k_{\text{Jb}}$ where the baryon Jeans wavenumber is

$$k_{\text{Jb}} = \left(\frac{3\Omega_m}{2a} \right)^{1/2} \frac{H_0}{c_b}, \quad (92)$$

with c_b being the baryon sound speed. The small residual ionization fraction persisting after the nominal recombination maintains the baryon temperature close to the microwave background temperature until $a \approx a_{\text{Tdec}} = 1/125$ yielding (for the standard cosmological parameters) $k_{\text{Jb}} = 252 \text{ Mpc}^{-1}$ for $a \ll a_{\text{Tdec}}$ and $k_{\text{Jb}} = 252\sqrt{a/a_{\text{Tdec}}} \text{ Mpc}^{-1}$ for $a \gg a_{\text{Tdec}}$. Thus, even before reionization, baryon perturbation growth is inhibited on scales $k > 252 \text{ Mpc}^{-1}$ or dark matter masses less than about $10^5 M_\odot$. Since we are mainly interested here in smaller scales, we will assume that baryons do not participate in gravitational instability. The CDM density perturbations therefore grow with time according to the $D_+(\tau)$ solution (82) with $f_b = \Omega_b/\Omega_m$. For $f_b = 0.168$, at $a = 1$ this results in an almost 50% reduction in linear growth compared with $f_b = 0$. Dark energy plays a

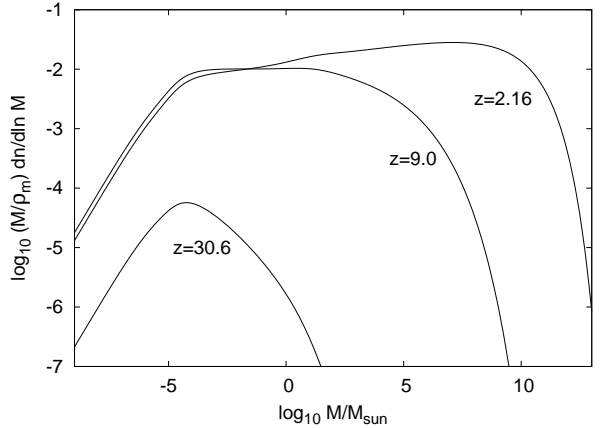


FIG. 12: Press-Schechter mass fraction for $n_s = 0.94$, $m_\chi = 100 \text{ GeV}$ and $T_d = 15.7 \text{ MeV}$, for several redshifts. Constant $(M/\rho_m)dn/d\ln M$ indicates equal mass is contained in objects whose masses span equal logarithmic mass intervals. The slight bump at $5 M_\odot$ is due to enhanced growth during electron pair annihilation. The growth on scales $M > 10^5 M_\odot$ has been underestimated by ignoring the boost given by infalling baryons.

role only at very late times. At $z = 2.16$, a cosmological constant with $\Omega_\Lambda = 0.74$ suppresses the growth of linear density perturbations by 2%.

Figure 12 shows the evolution of the mass function with redshift for plausible WIMP parameters. At $z = 31$ the peak of $Mdn/d\ln M$ occurs at $M \approx 2.3M_d$ (20 earth masses) but there may be numerous smaller objects. Indeed, the numerical results imply $d\sigma/d\ln M \propto -(M/M_d)^{2/3}$ for $M \ll M_d$. This follows from $W(kR)$ being an analytic function of $(kR)^2$ with $W(0) = 1$. For $R = 0$ the variance integral (88) converges because of the small-scale damping caused by kinetic decoupling. Thus, analyticity implies $\sigma^2 \propto C_1 - C_2(R/\tau_d)^2$ as $R \rightarrow 0$ where C_1 and C_2 are independent of filter radius $R \propto M^{1/3}$, hence $d\sigma/d\ln M \propto -(R/\tau_d)^2$ as $R \rightarrow 0$, or

$$\frac{dn}{d\ln M} \propto M^{-1/3}. \quad (93)$$

Given a smooth, symmetric window function, the number of small objects diverges but the mass contained in them converges.

These results for $M < M_d$ are uncertain because there are window functions $W(kR)$ that give a different result. For example, a sharp k -space filter, with $W(kR) = 1$ for $kR < \pi$ and zero otherwise, when combined with the free-streaming damping of $\nu(k, \tau)$, leads to an exponential cutoff instead of a power-law rise of $dn/d\ln M$ as $M \rightarrow 0$. However, a sharp k -space window gives rise to long-range oscillations in physical space, which seems unlikely to properly describe the local physics of dark matter halo formation.

The choice of window function represents an enormous simplification of the nonlinear dynamics of dark matter

halo formation. N-body simulations are needed to determine the correct mass function for $M < M_d$. Such simulations must fully resolve scales below the free-streaming damping length of 1.38 pc in the initial mass distribution. Cold dark matter caustics [20] are also likely to be important in the formation and dynamics of the smallest halos.

By redshift 9, RMS density perturbations become nonlinear and the small-scale mass distribution is nearly scale-invariant over 8 orders of magnitude of mass, $10^{-4.5} M_\odot$ to $10^{3.5} M_\odot$, reflecting the nearly scale-invariant ($n \approx -3$) character of the small-scale CDM density field. At later times larger objects build up by mergers of substructures as the effective spectral slope $n > -3$ on larger scales. The smallest-scale structure forms by almost sudden collapse as opposed to hierarchical clustering.

The results presented here do not include tidal destruction of small objects formed at high redshift. The survivability of earth-mass halos remains an open question [7, 18, 19]. The vast dynamic range of masses reflected in Fig. 12 provides an enormous challenge to numerical simulation methods attempting to determine the survival of the first forming halos [21].

VII. CONCLUSIONS

The small-scale transfer function of cold dark matter encodes rich information about WIMP physics. Were it possible to measure the power spectrum on scales below a solar mass, with precision similar to cosmic microwave background measurements on degree angular scales, we could hope to determine the WIMP mass and elastic scattering cross section with leptons by astrophysical means. This seems far-fetched because of the tremendous degree of nonlinear processing that has occurred since the first cold dark matter structures formed at a redshift about 50. However, if any of the smallest bound objects survive tidal stripping, they may produce an observable WIMP

annihilation signal [7] which provides a window into particle physics.

Moreover, the nearly scale-invariant structure predicted for dark matter fluctuations on mass scales below $10^4 M_\odot$ could affect the formation of larger-mass structures. This mass range is very difficult to study with standard numerical simulation methods.

While the present work has answered the question of how small-scale fluctuations in the WIMP distribution evolve during the linear stage of evolution, they raise new questions about nonlinear halo formation. If the Press-Schechter formalism with a local spatial filter (or analytic window function) correctly describes the formation of the smallest halos, then there is no minimum mass for WIMP microhalos; the mass function $dn/d\ln M \propto M^{-1/3}$ for $M < 10^{-4}(T_d/10 \text{ MeV})^{-3} M_\odot$. Most of the mass, however, is in larger clumps. Nonlinear evolution is likely to strongly modify the Press-Schechter distribution. Not only is tidal stripping important, but the Press-Schechter model is based on the assumption of hierarchical clustering, which breaks down on the small scales considered here.

The present paper has considered dark matter only in the form of a thermal relic, i.e. particles that were once in thermal equilibrium with the relativistic plasma of the early universe. The dark matter may be instead a nonthermal relic — the axion — which began its life as a Bose-Einstein condensate. The axion field begins oscillating after the QCD phase transition but is never collisionally coupled to the plasma. It would be interesting to investigate the smallest-scale structure in an axion dark matter model.

Acknowledgments

I thank Jon Arons for suggesting the Sonine polynomial expansion. This work was supported by the Kavli Foundation and by NSF grant AST-0407050.

[1] G. Bertone, D. Hooper, and J. Silk, *Phys. Rept.* **405**, 279 (2005).
[2] D. J. Eisenstein *et al.*, *Astrophys. J.* **633**, 560 (2005).
[3] G. Hinshaw *et al.*, *astro-ph/0603451*; L. Page *et al.*, *astro-ph/0603450*.
[4] S. Hoffman, D. J. Schwarz, and H. Stöcker, *Phys. Rev. D* **64**, 083507 (2001).
[5] V. Berezinsky, V. Dokuchaev, and Yu. Eroshenko, *Phys. Rev. D* **68**, 103003 (2003).
[6] A. M. Green, S. Hoffman, and D. J. Schwarz, *Mon. Not. R. Astron. Soc.* **353**, L23 (2004).
[7] J. Diemand, B. Moore, and J. Stadel, *Nature* **433**, 389 (2005).
[8] A. M. Green, S. Hoffman, and D. J. Schwarz, *JCAP* **0508**, 003 (2005).
[9] A. Loeb and M. Zaldarriaga, *Phys. Rev. D* **71**, 103520 (2005).
[10] S. Profumo, K. Sigurdson, and M. Kamionkowski, submitted to *Phys. Rev. Lett.* (*astro-ph/0603373*).
[11] C.-P. Ma and E. Bertschinger, *Astrophys. J.* **455**, 7 (1995).
[12] Ü. Seljak and M. Zaldarriaga, *Astrophys. J.* **469**, 437 (1996).
[13] S. Bashinsky and E. Bertschinger, *Phys. Rev. D* **65**, 123008 (2002).
[14] E. Bertschinger, *Astrophys. J.* **648**, in press (*astro-ph/0604485*).
[15] P. Meszaros, *Astron. & Astrophys.* **37**, 225 (1974).
[16] D. N. Spergel *et al.*, *astro-ph/0603449*.
[17] W. H. Press and P. Schechter, *Astrophys. J.* **187**, 425 (1974).
[18] V. Berezinsky, V. Dokuchaev, and Yu. Eroshenko, *Phys.*

Rev. D **73**, 063504 (2006).

[19] A. M. Green and S. P. Goodwin, astro-ph/0604142.

[20] P. Sikivie, I. I. Tkachev, and Y. Wang, Phys. Rev. Lett. **75**, 2911; D. Stiff and L. M. Widrow, Phys. Rev. Lett. **90**, 211301; R. Mohayaee and S. F. Shandarin, Mon. Not. R. Astron. Soc., **366**, 1217 (2006).

[21] J. S. Bagla and J. Prasad, Mon. Not. R. Astron. Soc., in press (astro-ph/0601320).

[22] Collisional damping before neutrino decoupling similarly justifies the neglect of the $m \neq 0$ modes for neutrinos in Ref. [11].

[23] Here, $\delta_L = \delta\rho_L/(\rho_L + p_L)$ is the number density perturbation in conformal Newtonian gauge; the energy density perturbation for the relativistic leptons is $\delta\rho_L/\rho_L = \frac{4}{3}\delta_L$.

[24] These fluid equations, like the Fokker-Planck equation from which they were derived, are correct only to leading order in T_L/m_χ . The corrections to (38a) and (38b) are $\dot{\Psi} \rightarrow \dot{\Psi} - \mathcal{H}\sigma$ and $\delta \rightarrow \nu = \delta + 3\mathcal{H}u$, respectively.

[25] For example, Eq. (47) describes the small-scale damping of fluctuations after recombination in a baryon-dominated universe.